

**Fixation-based Self-calibration for Eye Tracking in VR Headsets**

Ryusei Uramune, Sei Ikeda, Hiroki Ishizuka, and Osamu Oshiro

Osaka University, 1-3 Machikaneyama, Toyonaka, Osaka, Japan, 560-8531

*Email:* ruramune@acm.org

### Abstract

This study proposes a novel self-calibration method for eye tracking in a virtual reality (VR) headset. The proposed method is based on the assumptions that the user's viewpoint can freely move and that the points of regard (PoRs) from different viewpoints are distributed within a small area on an object surface during visual fixation. In the method, fixations are first detected from the time-series data of uncalibrated gaze directions using an extension of the I-VDT (velocity and dispersion threshold identification) algorithm to a three-dimensional (3D) scene. Then, the calibration parameters are optimized by minimizing the sum of a dispersion metrics of the PoRs. The proposed method can potentially identify the optimal calibration parameters representing the user-dependent offset from the optical axis to the visual axis without explicit user calibration, image processing, or marker-substitute objects. For the gaze data of 18 participants walking in two VR environments with many occlusions, the proposed method achieved an accuracy of  $2.1^\circ$ , which was significantly lower than the average offset. Our method is the first self-calibration method which is applicable to 3D environments without image-processing.

*Keywords:* Fixation detection, Self-calibration, Eye tracking, Virtual reality

## Fixation-based Self-calibration for Eye Tracking in VR Headsets

### Introduction

In virtual and augmented reality (VR/AR), eye tracking has been shown to be effective not only for offline applications, such as psychological analysis and usability evaluation, but also for various online applications, including foveated rendering (Meng et al., 2018), precise ocular parallax displays (Konrad et al., 2020; Krajancich et al., 2020), depth of field rendering (Orisaka & Okatani, 2016), auto-focus displays (Padmanaban et al., 2019), and object selection (Mardanbegi et al., 2019). As of 2023, camera-based eye-tracking is still widely used as a standard feature in VR/AR head-mounted displays (HMDs), as exemplified by FOVE, HTC Vive Pro Eye, Magic Leap, and Microsoft HoloLens2. Most devices need to be calibrated before use to obtain highly accurate line of sight. In the above applications, the accuracy of gaze measurement can be one of the main factors that determine the performance of the applications. For example, in foveated rendering, low accuracy in gaze measurement increases rendering cost by enlarging the area of detail to be rendered; in object selection, it becomes difficult to select small objects.

The principle of eye tracking calibration is strongly based on the human visual system. The human eyeball obtains a clear image by rotating to capture a target at the fovea, a spot on the retina where the distribution density of cones, the photoreceptors mainly related to bright vision, is the highest. The line passing through the fovea and the center of the lens is called the visual axis. In contrast, an eye tracker can directly observe some feature related to the optical (or geometric) axis, which is the line passing through the center of the eyeball rotation and the center of the pupil. The visual axis is typically offset from the optical axis by about  $4^\circ$  to  $7^\circ$  (Carpenter, 1988). According to literature (Abass et al., 2018), the offset has non-negligible individual differences, with a maximum difference of  $19.57^\circ$  in the horizontal direction and  $16.25^\circ$  in the vertical direction. Therefore, in order to obtain accurate gaze directions by observing the eye balls, a calibration to estimate the offset cannot be avoided.

In traditional calibration methods, several reference markers are presented to the user, and

the user is asked to gaze at each marker individually, both before and sometimes after gaze measurements. Such calibration inhibits VR experiences. After the calibration, many state-of-the-art eye trackers maintain accuracy, even when the head is moved in relation to the device. This ability depends not so much on the calibration method as on the gaze estimation model. As summarized in the next section, various gaze estimation models exist and can be divided into four categories: two-dimensional (2D) regression models, three-dimensional (3D) eye model-based models, appearance-based models, and head-correlation models (Hansen & Ji, 2010; Kar & Corcoran, 2017). The former three models are based on eye observations and require calibration. The head-correlation models are challenging approach to estimate the visual axis from head motion (Hu et al., 2019, 2020; Li et al., 2013) without the use of eye trackers. Although they do not require the estimation of offsets, they are inaccurate.

Self-calibration (also called automatic or implicit calibration) can be defined as a technology that estimates the individual offset angles from other information, such as scene images or time-series data of the optical axis. Self-calibration can reduce total experimental time in offline applications. In online applications, the eye tracker can be calibrated at any time as needed. Self-calibration methods can be divided into saliency-based (Chen & Ji, 2015; Liu et al., 2020; Shi et al., 2020; Sugano et al., 2013; K. Wang et al., 2016), smooth pursuit-based (Muraier et al., 2018; Tamura & Takemura, 2020), and scene model-based methods (Maio et al., 2011; Miki et al., 2016; Model & Eizenman, 2010b; Nagamatsu, Sugano, et al., 2010; Nagamatsu et al., 2013; Uramune et al., 2021; K. Wang & Ji, 2018), as described in detail in the next section. These approaches vary in terms of finding the visual axis cues. Most methods compute the offset angles from the cues obtained by analyzing scene images or scene models over a set amount of time. Once the offsets are obtained, the optical axis can be directly converted to the visual axis. In particular, scene model-based methods have been reported to achieve higher accuracy than the other methods. However, no cases of successful calibration using this type of method in 3D environments in which the user can freely move have been reported to date. Moreover, the conventional scene model-based methods are limited to flat monitors (Maio et al., 2011; Miki

et al., 2016; Model & Eizenman, 2010b; Nagamatsu, Sugano, et al., 2010; K. Wang & Ji, 2018), objects at infinity (Nagamatsu et al., 2013), or differentiable curved surfaces (Uramune et al., 2021).

In this study, we propose a self-calibration method for eye tracking in VR headsets. The purpose of this paper is to show the following assertions:

- I. The proposed method is the only self-calibration method applicable in 3D environments where scene images cannot be acquired (see *Related Work*).
- II. The proposed method takes advantage of the fact that many lines of sight during fixation intersect near a single point on the object surface even when the user's head is moving. The proposed method does not require scene images or specific objects such as markers (see *Method*).
- III. The proposed method can calibrate the eye tracker with an accuracy of about 2 degrees in a situation where the user is walking and moving in a VR environment with many objects in view, including various textures and occlusions (see *Experiments*).

The proposed method assumes the head position and scene model as known information and estimates the calibration parameters using the points of regard (PoRs) during fixational eye movements. Therefore, this method can be classified as a scene model-based method. The definition of fixation varies among researchers and communities (Hessels et al., 2018). In this study, as in previous studies (Massé et al., 2018; Steil et al., 2018), we define fixation as a state in which the PoRs are densely packed in the object coordinates for a certain period of time. According to this definition, even when the object being gazed at or the head is in motion, the eyes track a single point on the object by smooth pursuit eye movements during a fixation. Thus, in principle, our method is also similar to smooth pursuit-based methods except that the object being tracked must be identified.

As shown in Fig. 1, our method is based on the assumptions that the PoRs in each fixation are densely concentrated on an object surface if the eye tracker is accurately calibrated and that the dispersion of the PoRs in each fixation increases when the gaze measurement contains large

errors. Evaluating the dispersion of PoRs is similar to evaluating whether the thinnest part of the line-of-sight bundle is near the object surface. The proposed method is inspired by multi-view geometry techniques such as multi-view stereo and camera self-calibration, where the user's view is represented by a pinhole camera model. In such multi-view techniques, rays from multiple cameras to the same point intersect on the object surface as a clue to estimate some parameter. It is well known that the rotation of the camera is generally irrelevant, and the baseline distance between different cameras affects the accuracy. The same is true for our method, where simply rotating the user's head at the same point is not sufficient for calibration; the head must be translating during the short period of time that fixation occurs.

The proposed method has two steps. First, it detects fixations from the time-series data of uncalibrated gaze directions. We extend an existing I-VDT (velocity and dispersion threshold identification) (Komogortsev & Karpov, 2013) algorithm suitable for fixation detection in 3D scenes. Second, the method estimates calibration parameters by minimizing a novel cost function. The cost function is designed based on the reprojection errors of the PoRs. The reprojection errors are defined on the image plane of the pinhole camera representing the user's field of view, which is named a scene camera in this paper (see Fig. 1).

### **Related Work**

In *Gaze Estimation Models*, we first briefly summarize the various models for gaze estimation from sensing data and show the types of calibration parameters required for each model. Then, in *Self-calibration Methods*, we explain the existing methods for automatically estimating such parameters and clarify the differences between these and the proposed method. Finally, in *Fixation Detection Algorithms for 3D Scenes*, we describe the existing fixation detection algorithms and their problems, as the results of fixation detection significantly affect calibration accuracy (see *Dependence on Initial Parameters*).

### **Gaze Estimation Models**

As mentioned above, existing gaze estimation models can be divided into four types: 2D regression models, 3D eye models, appearance models (Hansen & Ji, 2010), and head-correlation

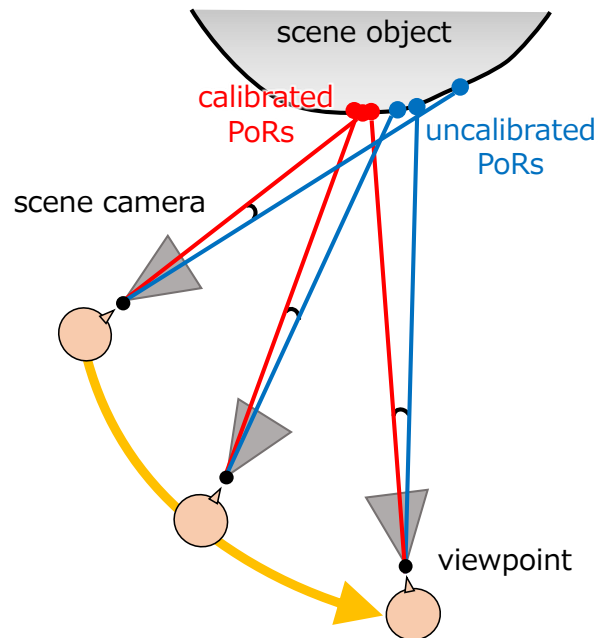


**Figure 1**

*Principle of the proposed fixation-based calibration method. During a fixation, human eyeballs move so that the PoRs are concentrated around a single point, even if the head moves. We applied this characteristic and the corresponding multi-view geometry to the self-calibration of an eye tracker.*

models. This section discusses the conventional gaze estimation models and how they are not capable of determining the visual axis with sufficient accuracy without the provision of individual offset angles.

### ***2D Regression Models***

2D regression models map 2D coordinates, including the pupil center and glint positions (reflections of light sources), in an eye image to a two-degree-of-freedom (DoF) gaze direction. As mapping functions, polynomials (Stampe, 1993; K. Wang et al., 2016; White et al., 1993) are often used as Taylor approximations of arbitrary transformation functions (Blignaut, 2013). In addition to polynomials, machine learning models such as Gaussian process interpolation (Hansen et al., 2002), neural networks (Zhu & Ji, 2004), and support vector machines (Zhu et al., 2006) are used.

Calibration of 2D regression models requires numerous pairs of pupil center, approximately corresponding to the optical axis, and marker position, corresponding to the visual axis. The regression coefficients in the calibration are the coefficients of the mapping function. These coefficients contain information on the pose of the eyeball relative to the camera and the offset angles, which cannot be separated. Therefore, in 2D regression models, recalibration is necessary when the user's head moves relative to the eye tracker, even if the same user is continuously using the same tracker. In addition, calibration generally requires a sufficient number of markers to cover the entire field of view (FOV). In our experiments, we used the calibration results from a polynomial-based 2D regression as a control condition.

### ***3D Eye Models***

Calibration of 3D eye models determines the optical axis through feature detection on eye images. Most of the eye model-based approaches approximate the surface shape of the eyeball using a combination of two spheres (Villanueva et al., 2007; J. G. Wang et al., 2005); a few of them use an ellipsoid (Beymer & Flickner, 2003) or a solid of revolution around the optical axis (Nagamatsu, Iwamoto, et al., 2010). The optical axis can be determined using one camera and a few point light sources, allowing for head movement (Guestrin & Eizenman, 2006). Our method adopts two DoF offset angles as the calibration parameters of the sphere model.

For calibration, most 3D models use one (Nagamatsu et al., 2008; J. G. Wang et al., 2005) or two (Beymer & Flickner, 2003; Chen & Ji, 2015; Nagamatsu, Iwamoto, et al., 2010; Villanueva et al., 2007) DoF offset angles between the optical and visual axes. In rare cases, models that require the estimation of three parameters (one DoF offset between the optical and visual axes, radius of corneal curvature, and distance between the pupil center and the center of corneal curvature) also exist (Nagamatsu, Iwamoto, et al., 2010; Nagamatsu et al., 2021). In summary, each model has different individual parameters, which must be estimated for each user calibration. Our method adopts two DoF offset angles as the calibration parameters.

### *Appearance Models*

In appearance models, an eye image is used without manually designed feature extraction and machine learning to directly output the gaze direction. Several learning algorithms have been considered, including neural networks with three layers (Baluja & Pomerleau, 1993; Stiefelhagen et al., 1997; Xu et al., 1998), manifold learning (Tan et al., 2002), Gaussian processes (Williams et al., 2006), and deep neural networks (Krafka et al., 2016; Zhang et al., 2015). A complete description of the state-of-the-art convolutional neural network-based methods, summarized in (Akinyelu & Blignaut, 2020), lies outside the scope of this study.

The performance of machine learning depends on the training dataset. For these techniques to be used as calibration-free gaze estimators, they must be trained on a dataset that does not include the user's data. However, individual differences in the position of the fovea cannot be predicted from the appearance of the eyeball. For high-accuracy estimation of the individual visual axis, training with data specific to each individual user (Stiefelhagen et al., 1997; Zhang et al., 2015) or compensating for accuracy using an offset table (Baluja & Pomerleau, 1993; Xu et al., 1998) that maps the amount of correction for each user is necessary. Either of these requires at least one explicit operation similar to user calibration. In general, appearance models are less accurate than 3D or regression models (Kar & Corcoran, 2017).

### *Head-correlation Models*

Head-correlation models are the challenging techniques that estimate the visual axis without observation of eyes (Hu et al., 2019, 2020; Li et al., 2013). These models commonly estimate the direction of the visual axis by combining the head-eye coordination and the scene points that the user is likely to pay attention to. The fingertip position (Li et al., 2013), saliency map (Hu et al., 2019, 2020), and moving objects (Hu et al., 2020) are used as cues to identify such scene points. Calibration is not required for these models, as the visual axis is estimated frame by frame. In principle, the offset can be determined by combining the visual axis estimated by these models and the optical axis obtained from the eye tracker. That is, these models are applicable for self-calibration if the estimation accuracy is sufficiently high. Unfortunately, the

reported estimation errors exceed  $7^\circ$  (Hu et al., 2019, 2020; Li et al., 2013), which is an angle as large as or larger than the typical offset.

### **Self-calibration Methods**

Self-calibration is a technique that estimates the offset angles without the placement of any special objects or without the user being aware of the process. Table 1 summarizes the features of conventional self-calibration methods. Three main approaches to self-calibration exist: saliency-based, smooth pursuit-based, and scene model-based methods.

#### ***Saliency-based Methods***

Saliency-based methods extract the global maximum position of the saliency in the FOV as the visual axis. Because a saliency map generated from a single-frame scene image is multi-modal, most saliency-based methods try to improve accuracy by accumulating multiple frames of saliency maps. However, the accuracy of most methods with simple accumulation is limited to about  $3^\circ$  (Chen & Ji, 2011; Sugano et al., 2013). To further improve accuracy and efficiency, several methods limit the scenes or frames to be accumulated to only those with low entropy (Chen & Ji, 2015; K. Wang et al., 2016), with faces (Hiroe et al., 2019), or with gaze data of many other people looking at the same scene (Alnajar et al., 2017). However, such approaches limit the applications or situations. In all of the studies presented above, experiments were conducted with the participants seated in front of a flat monitor.

For 3D scenes, two methods have been proposed to calibrate a head-mounted eye tracker while the user is freely walking in a real (Liu et al., 2020) or VR (Shi et al., 2020) environment. To more accurately detect the maximum saliency, these methods adopt multi-frame accumulation considering the 3D environments. Liu et al. (Liu et al., 2020) limited the area of saliency to the object area, and Shi et al. (Shi et al., 2020) projected the saliency map of one eye onto the other eye via the 3D shape of the scene. Despite these improvements, accuracy of about  $3^\circ$  or worse has been reported (Liu et al., 2020; Shi et al., 2020). In addition, acquiring scene images to compute the saliency map frequently incurs additional high computational costs in VR systems.

**Table 1***Comparison of Self-calibration Methods*

Methods <sup>1</sup>	Base approaches	Target scene	Head pose	Scene image	Accuracy <sup>2</sup>
Sugano et al., 2013	saliency	flat monitor	fixed	necessary	3.5°
Chen and Ji, 2011, 2015	saliency	flat monitor <sup>3</sup>	fixed	necessary	3.4°
K. Wang et al., 2016	saliency	flat monitor <sup>3</sup>	free	necessary	1.0°/1.4°
Alnajar et al., 2017	saliency	flat monitor	free	necessary	4.2°
Hiroe et al., 2019	saliency	flat monitor <sup>4</sup>	fixed	necessary	1.71°
Liu et al., 2020	saliency	arbitrary scene	free	necessary	3.7°/4.0°
Shi et al., 2020	saliency	arbitrary scene	free	necessary	3°–4°
Murauer et al., 2018	smooth pursuit	arbitrary scene <sup>5</sup>	free	necessary	6.17°
Tamura and Takemura, 2020	smooth pursuit	arbitrary scene <sup>5</sup>	free	necessary	—
Nagamatsu, Sugano, et al., 2010	scene model	flat monitor	free	unnecessary	1.58°
Model and Eizenman, 2010a, 2010b	scene model	flat monitor	free	unnecessary	1.3°
Maio et al., 2011	scene model	flat monitor	free	unnecessary	2.4°–8.9°
Nagamatsu et al., 2013	scene model	infinity	free	unnecessary	0.2°
Miki et al., 2016	scene model	flat monitor	free	unnecessary	0.5° <sup>6</sup>
K. Wang and Ji, 2018	scene model	flat monitor	free	unnecessary	1.3°
Uramune et al., 2021	scene model	continuous surface	free	unnecessary	1.29°
<b>Proposed method (optical axis)<sup>7</sup></b>	<b>scene model</b>	<b>arbitrary scene</b>	<b>free</b>	<b>unnecessary</b>	<b>2.12°</b>
<b>Proposed method (visual axis)<sup>8</sup></b>	<b>scene model</b>	<b>arbitrary scene</b>	<b>free</b>	<b>unnecessary</b>	<b>1.20°</b>

1. The self-calibration methods that do not require real or virtual markers are listed.
2. The accuracy evaluation methods are not standardized. Only a rough comparison is meaningful.
3. The scene is limited to a static scene image with low entropy.
4. The face of a person must be displayed.
5. Smooth pursuit-based methods rely on a few objects that move in correlation with the eye.
6. Real gaze data were not used in the experiments.
7. The optical axis was used as the initial calibration parameter for fixation detection.
8. The visual axis was used as the initial calibration parameter for fixation detection.

***Smooth Pursuit-based Methods***

Smooth pursuit-based methods have emerged as PoR estimation techniques without user calibration. They can also be applied to self-calibration after PoRs with high accuracy are obtained (Velloso et al., 2016). Such methods can identify the target of the user's gaze based on the similarity between the motion of the eye and the motion of the target in the scene images.

Once the target is determined, the offset can be calculated by considering one point on the target object as the direction of the visual axis (Murauer et al., 2018; Tamura & Takemura, 2020).

Smooth pursuit-based methods assume that it is possible to identify a single image point that moves on a similar trajectory as the PoR. This requires the target object to be small, and no other object must have the same movement. The accuracy of these methods has been reported to be around  $4^\circ$  to  $6^\circ$  (Murauer et al., 2018). These methods are similar in principle to our proposed method, which utilizes the PoRs during smooth pursuits caused by fixation; however, the proposed method does not require the identification of the object at which the user is gazing.

### ***Scene Model-based Methods***

In scene model-based methods, the optical axis direction and the scene shape are used to determine the visual axis direction. Nagamatsu et al. proposed a method to calculate a single PoR as the midpoint between the two intersections of the optical axes of both eyes on a monitor plane (Nagamatsu, Sugano, et al., 2010). This method is equivalent to estimating the horizontal component of the offset between the optical and visual axes but cannot correct for the vertical component. Model et al. generalized this method to estimate the two DoF offset angles for each eye, minimizing the distance between the two intersections of the optical axes of both eyes on the planar screen (Model & Eizenman, 2010b). This generalized method has been improved to make the solution more stable (Miki et al., 2016) and efficient (S. Wang et al., 2016). In addition to the constraint of coincidence of the intersections of the two eyes' visual axes (Nagamatsu, Sugano, et al., 2010), other constraints have been indicated. Examples include the constraint that the PoR is within the screen and the range of the offset angles (Maio et al., 2011), and the constraint that the results of the different methods coincide (K. Wang & Ji, 2018). In the methods mentioned above, however, the scene is limited to a flat monitor (Model & Eizenman, 2010b; Nagamatsu, Sugano, et al., 2010) or to infinity (Nagamatsu et al., 2013).

Our proposed method can be classified as a scene model-based method in the sense that it assumes the 3D shape of the scene, which is inevitably available for VR applications. Our previous work has also proposed a self-calibration method using the variance of PoRs on the

surface of a 3D scene model (Uramune et al., 2021). However, although this method is similar to the proposed method, it does not support scenes with discontinuous depths or occlusions. From the foregoing discussion in *Self-calibration Methods*, it is evident that Assertion I has been substantiated.

### **Fixation Detection Algorithms for 3D Scenes**

In this section, we first review the fundamentals of fixation detection; next, we provide a overview of detection algorithms. During fixation, the gaze remains stationary for at least 80–100 ms within  $2^\circ$ – $5^\circ$  of the central visual field (Hansen & Ji, 2010; Manor & Gordon, 2003). When the target object or the head is moving, fixation is maintained by smooth pursuit eye movements and the vestibulo-ocular reflex. Rapid eye movements between two successive fixations are called saccades, which have velocities of 100 – 700  $^\circ$ /s (Kar & Corcoran, 2017). A detailed explanation of eye movements is beyond the scope of this paper. Interested readers may refer to (Carpenter, 1988) for a detailed description.

The results of fixation detection depend on the detection algorithm and parameters such as threshold values (Blignaut, 2009; Shic et al., 2008). Previous studies (Hooge et al., 2022; Manor & Gordon, 2003; Poole & Ball, 2006) reported that the number of fixations and the average fixation time are significantly influenced by changes in the algorithm and threshold values. In some cases, these changes affect the conclusions of later analyses (Shic et al., 2008). The optimization results of the proposed method also depend on the results of fixation detection, as shown in *Dependence on Initial Parameters*. Thus, here we explain the need for algorithms suitable for fixation detection in 3D scenes.

Fixation detection algorithms from time-series gaze direction data can be divided into two main categories based on the reference coordinate systems: scene camera coordinate system and object coordinate system (Salvucci & Goldberg, 2000). The scene camera coordinate system involves a coordinate system fixed to the scene camera— that is, the user’s head. If the head is fixed, there is little difference between the two systems; otherwise, their properties significantly differ. The algorithms using scene camera coordinates takes advantage of the fact that the angular

velocity of the gaze during fixation is sufficiently slow compared with that of the saccades. A typical algorithm is I-VT (velocity threshold identification) (Salvucci & Goldberg, 2000), which identifies gaze directions as a fixation if the angular velocity of successive gaze directions in the scene camera coordinate system is below a certain threshold. This algorithm has a wide range of applications because it does not require object information and is almost independent of the initial calibration parameters. However, it tends to produce more misdetections than algorithms using object coordinates (Salvucci & Goldberg, 2000). This may be even more likely when head rotation occurs.

The algorithms that use object coordinates are based on the fact that the dispersion of PoRs during a fixation is small. A typical algorithm is I-DT (dispersion threshold identification) (Salvucci & Goldberg, 2000), which identifies PoRs as a fixation if the PoRs in the object coordinate system are within a certain range for a certain period of time or longer. This algorithm is less prone to false positives from other eye movements. Larsson et al. have tried to develop an intermediate algorithm that detects fixations by thresholding the angular velocity in the world coordinate system with the head pose without object shapes (Larsson et al., 2016). This method allows head movements and arbitrary scenes. However, a single velocity threshold can incorrectly detect fixation in situations where head movement is large, such as in our VR environments. I-VDT (Komogortsev & Karpov, 2013) simply combines a velocity threshold with a dispersion threshold to achieve the intermediate properties of I-DT and I-VT. In principle, I-DT and I-VDT are expected to be insensitive to both rotation and translation of the head, but neither of them is applicable to arbitrary scenes, as the dispersion of PoRs is defined only on a flat monitor.

Only few methods for detecting fixation for scenes with large head movements and arbitrary shapes have been proposed (Jurado et al., 2020; Steil et al., 2018). One is to use pattern matching with the similarity of scene image patches around the PoRs to detect fixations (Steil et al., 2018). The disadvantages of this method are misdetections in texture-less and repeated-pattern regions and bandwidth-consuming image capturing. Another method is to define

the dispersion on a 3D object (Jurado et al., 2020). This method is similar to the algorithm we employ. Although this method has been recently published, various studies have clarified the properties of I-DT and I-VT. Therefore, in this study, we further extend the I-VDT method, which combines both I-DT and I-VT, to a 3D environment. The details of the algorithm and its relationship with I-DT and I-VT are explained in the next sections.

## Method

### Preliminary Information

We first present our assumptions and define the variables necessary to the explanation of our proposed method. In this method, a single virtual scene camera (pinhole camera) representing the user's cyclopean eye is used for all our gaze processing, although different stereoscopic images are presented to both eyes on the HMD. Assuming that the focal length of the scene camera is 1, an arbitrary gaze direction can be expressed as  $\mathbf{g} = [u, v, 1]^T$  using the homogeneous representation of the 2D coordinate  $[u, v]^T$  on the image plane. If the position of a PoR represented as an object coordinate  $\mathbf{X}$ , the projection onto the scene camera image yields the following equation:

$$\mathbf{g} = \pi(\mathbf{X}), \quad (1)$$

where  $\pi$  is the mapping from the object coordinate  $\mathbf{X}$  to the image coordinate.  $\pi$  can be obtained at the same acquisition rate as the gaze measurement. Conversely, if  $\mathbf{X}$  is the point where the extension of the line of sight in the direction  $\mathbf{g}$  first collides with the object surface, it is expressed as  $\mathbf{X} = \pi^{-1}(\mathbf{g})$  using the inverse projection  $\pi^{-1}$ .

The inputs in this method include a set of gaze directions  $\{\mathbf{g}_i\}$ , the position and orientation of the HMD (corresponding to the projection  $\{\pi_i\}$  or inverse projection  $\{\pi_i^{-1}\}$ ) at  $M$  discrete time frames ( $i = 1, 2, \dots, M$ ), and a 3D environment model. The model's texture is displayed but not used for the computation of the proposed method. In the general 3D eye model described in *Gaze Estimation Models*, the transformation from the optical axis  $\mathbf{g}_{\text{opt}}$  to the visual

axis  $\mathbf{g}_{\text{vis}}$  is presented by the following equation:

$$\mathbf{g}_{\text{vis}} \propto f(\mathbf{g}_{\text{opt}}; \boldsymbol{\theta}_{\text{offset}}), \quad (2)$$

$$= \begin{bmatrix} 1 & 0 & 0 \\ 0 & \cos \beta_0 & \sin \beta_0 \\ 0 & -\sin \beta_0 & \cos \beta_0 \end{bmatrix} \begin{bmatrix} \cos \alpha_0 & 0 & \sin \alpha_0 \\ 0 & 1 & 0 \\ -\sin \alpha_0 & 0 & \cos \alpha_0 \end{bmatrix} \mathbf{g}_{\text{opt}}, \quad (3)$$

where  $\propto$  is the symbol for proportionality in the homogeneous representation, indicating that both sides are equal in Cartesian representation.  $\boldsymbol{\theta}_{\text{offset}} = [\alpha_0, \beta_0]$  is the offset angle addressed in Section 1.  $\alpha_0$  and  $\beta_0$  are the horizontal and vertical components of the offset angle, respectively.

In this model, the axis directly measured by the eye tracker is not necessarily the optical axis, as long as it satisfies Equation (3), i.e., the axis only needs to be fixed to the eyeball.

Although strictly speaking, the axis must pass through the center of rotation of the eyeball, but if the scale of the environment is large enough, a relatively small discrepancy between the center of rotation and the axis can be ignored.

The calibration parameters to be obtained as the final output are the estimated offset angles in the 3D eye model. The calibration function  $f$  mapping  $\mathbf{g}_{\text{opt}}$  to an arbitrary direction  $\mathbf{g}$  can be expressed as the following equation:

$$\mathbf{g} \propto f(\mathbf{g}_{\text{opt}}; \boldsymbol{\theta}), \quad (4)$$

where  $\boldsymbol{\theta} = [\alpha, \beta]$  is a set of two arbitrary calibration parameters.  $\alpha$  and  $\beta$  are the horizontal and vertical rotation angles of the gaze direction, respectively.

The proposed method estimates the calibration parameter  $\boldsymbol{\theta}$  using the above input information in two major steps: fixation detection and calibration parameter optimization. In the next section, we explain in detail the extended I-VDT algorithm for fixation detection. Then, in *Optimization of Reprojection Errors*, we introduce the reprojection errors and describe the optimization method using these errors.

## Fixation Detection

Fixations are detected using the I-VDT algorithm extended to a 3D environment. Our extended I-VDT (referred to as 3D I-VDT) combines I-VT with the extended I-DT (referred to as 3D I-DT) to 3D scenes; also, the original I-VDT is a combination of I-VT and I-DT. Therefore, this section describes the I-VT, 3D I-DT, and 3D I-VDT in order.

These algorithms generally adopt a moving window for successive data frames to check for a fixation candidate. The window has minimum  $m$  frames that must satisfy certain conditions.  $m$  can be determined by the minimum fixation time  $T_{th}$  and the sampling rate  $S_r$ :

$$m = S_r T_{th}. \quad (5)$$

In any algorithm, the movement of the window is as follows. Initially, the window contains  $m$  frames. Let  $\mathbf{G}$  be an index set of the window, which is initially set as  $\mathbf{G} = \{i - m + 1, \dots, i\}$ , where  $i$  is the current frame. If some criterion computed from the gaze data in the window satisfies a certain condition, the window is expanded to include the next frame, i.e.,  $\{i - m + 1, \dots, i + 1\}$ . The window continues to expand as many times as the condition is satisfied. If the condition is no longer satisfied owing to the window expansion, the gaze data in the window right before the expansion is labeled as the same fixation. The window is shrunk to the original size  $m$  and jumped so that the index set is updated to  $\mathbf{G} = \{i + 1, \dots, i + m\}$ . If the condition is not satisfied without the expansion, all the frames in the window are identified as not a fixation; the window slides by one frame. Hereafter,  $k$  is used as the local index representing one frame in the window.

### *Algorithm of I-VT*

The I-VT algorithm (Salvucci & Goldberg, 2000) detects fixations based on the angular velocity for each gaze direction. In implementation,  $\{\mathbf{g}_k\}$  is categorized as a fixational gaze if any gaze direction  $\mathbf{g}_k$  satisfies the following equation.

$$\frac{\mathbf{g}_{k-1} \cdot \mathbf{g}_k}{|\mathbf{g}_{k-1}| |\mathbf{g}_k|} > \cos \phi_{th} \quad (k - 1, k \in \mathbf{G}), \quad (6)$$

where  $\phi_{th}$  is the angle threshold, and ‘ $\cdot$ ’ represents the inner product.

### *Algorithm of 3D I-DT*

The original I-DT algorithm (Salvucci & Goldberg, 2000) calculates a dispersion of the PoRs from the gaze data contained in the window  $G$ . Dispersion can be calculated using several methods, such as the distance between the most distant PoRs, the largest distance from the center of the PoRs to any PoR, and the standard deviation (Blignaut, 2009). The conventional I-DT is limited to a flat monitor, and the dispersion of the PoRs is calculated on a 2D plane.

To extend the I-DT to 3D scenes with head movements, the 3D I-DT calculates a 2D dispersion after the PoRs are projected onto a scene camera. For the projection, we select a center camera from the multiple scene cameras corresponding to window  $G$ . The center camera represents an average head posture. Because the window size is about a few hundred milliseconds and the change in head posture is small, a camera with an average gaze direction is selected as the center camera. For gaze directions  $\{g_k | k \in G\}$ , the selection criterion to determine the  $k_c$ -th camera as the center camera is as follows:

$$g'_k \propto R_k^{-1} g_k, \quad (7)$$

$$k_c = \arg \min_{k \in G} |g'_k - \bar{g}'|, \quad (8)$$

where  $\bar{g}'$  is the sample mean of  $\{g'_k | k \in G\}$ .  $g_k$  and  $g'_k$  are the gaze direction vectors expressed in the scene camera and object coordinates, respectively, and both are normalized so that their magnitude is 1.  $R_k$  is the rotation matrix from the scene camera coordinates to the object coordinates and is the rotational component of the inverse projection function  $\pi_k^{-1}$ .

The dispersion is evaluated with reprojection errors on the image plane of the center camera in 3D I-DT. Fig. 2 shows a reprojection error as the 2D distance between a projected PoR and the average point of all the PoRs on the center camera image. The 3D I-DT algorithm first calculates the 3D position of the PoR  $X_k$  as the inverse projection of the gaze direction  $g_k$ :

$$X_k = \pi_k^{-1}(g_k). \quad (9)$$

Next, the PoR  $X_k$  is projected to the center camera to obtain the reprojection point  $x_k$  using the

following equation:

$$\mathbf{x}_k = \pi_{k_c}(\mathbf{X}_k). \quad (10)$$

This projection prevents extremely large evaluation values even for PoRs scattered in the depth direction near the occlusion edge of the object. Finally, the gaze directions  $\{\mathbf{g}_k | k \in \mathbf{G}\}$  are labeled as a single fixation if the reprojected PoRs satisfy the following equation:

$$\arg \max_{k \in \mathbf{G}} |\mathbf{x}_k - \bar{\mathbf{x}}_G|^2 < D_{\text{th}}, \quad (11)$$

where  $\bar{\mathbf{x}}_G$  is the sample mean of  $\{\mathbf{x}_k | k \in \mathbf{G}\}$ , and  $D_{\text{th}}$  is the dispersion threshold.

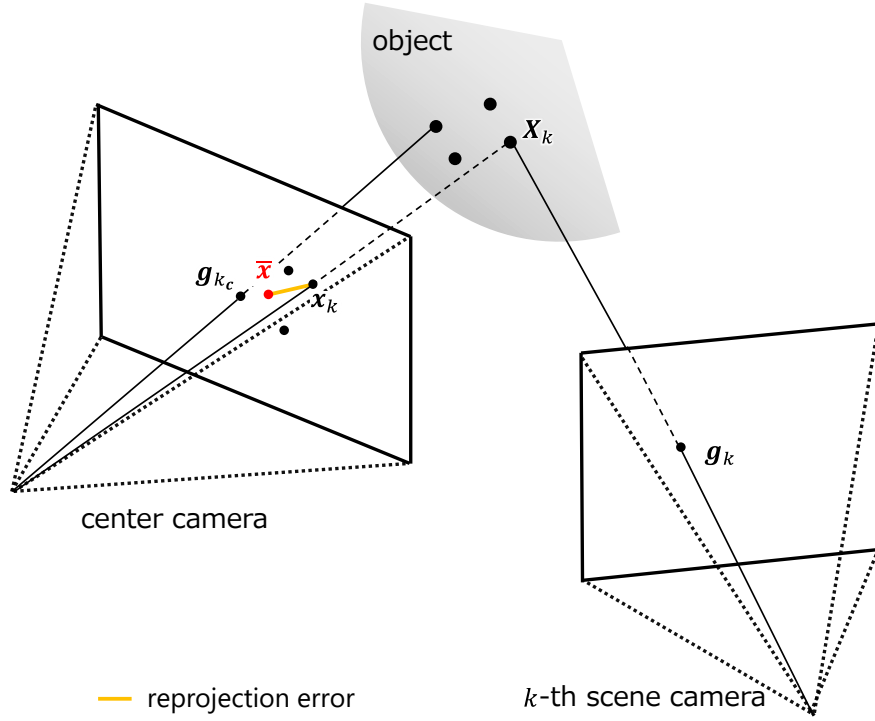
### ***Algorithm of 3D I-VDT***

The I-VDT algorithm is a fixation detection algorithm that combines I-VT and I-DT. 3D I-VDT uses both a velocity threshold  $\phi_{\text{th}}$  and a dispersion threshold  $D_{\text{th}}$ . The same moving window as in 3D I-DT is used. If all the gaze directions in the window simultaneously satisfy both Equations (6) and (11), I-VDT categorizes the gaze directions  $\{\mathbf{g}_k | k \in \mathbf{G}\}$  as a fixation.

Both 3D I-DT and 3D I-VDT algorithms work equivalently to the original I-DT and I-VDT, respectively, under the fixed head condition. For simplicity, we abbreviate below the 3D I-DT and 3D I-VDT algorithms as I-DT and I-VDT, respectively, unless there is a risk of misunderstanding. In addition, let  $N$  fixations be obtained using the abovementioned I-VDT algorithm and  $\mathbf{G}_j$  be the set of frame numbers corresponding to the  $j$ -th detected fixation that comprises of  $M_j$  frames. Hereafter, we call each set a fixation cluster.

### **Optimization of Reprojection Errors**

In the first part of this section, we define the optimization metric, reprojection error; in the second part, we describe the optimization method. As mentioned in *Fixation Detection*, the reprojection error is defined on the center camera that is representative of each fixation cluster, as in Fig. 2. Although the definition is the same, and we refer to the same figure as in the description of fixation detection, the projection and inverse projection in the optimization are slightly different from those in I-DT: the parameters in the process of optimization are used for both projection and back projection.

**Figure 2**

*Reprojection errors. In the proposed method, the calibration parameters are estimated by optimizing a cost function based on the reprojection errors.*

The optimization metric is determined as follows. First, we select the  $k_c$ -th camera as the center camera from the  $M_j$  scene cameras belonging to the  $j$ -th fixation cluster using Equations (7) and (8). The reprojection error function  $E_j$  of the  $j$ -th fixation cluster  $G_j$  is the mean of squares of the reprojection errors.  $E_j$  is defined by the following equation:

$$E_j(\theta) = \frac{1}{M_j} \sum_{k \in G_j} |x_k - \bar{x}_{G_j}|^2, \quad (12)$$

where  $\bar{x}_{G_j}$  is the sample mean of  $\{x_k | k \in G_j\}$ . That is to say,  $E_j$  is equivalent to the 2D variance of the set of the PoRs  $\{X_i\}$  on the image plane. The 3D point  $X_k$  is calculated as the inverse-projection point of the calibrated gaze direction  $g_k$ :

$$X_k = \pi_k^{-1}(f(g_k; \theta)). \quad (13)$$

Thus, we can find  $E_j$  of cluster  $G_j$  is a function of  $\theta$ .

Via optimization, the sum of the reprojection error functions for multiple fixation clusters is minimized. The cost function simultaneously minimizes the reprojection error function for  $N$  fixation clusters to estimate the optimal calibration parameters  $\hat{\theta}$ :

$$\hat{\theta} = \arg \min_{\theta} \sum_{j=1}^N E_j(\theta). \quad (14)$$

This function has multiple local minima. Therefore, a global optimization algorithm is required. In our method, differential evolution (Storn & Price, 1997) is applied as one possible approach for finding optimal parameters. This optimization method is a type of evolutionary computation algorithm that does not require differentiability or convexity assumptions for the objective function and can search for the global optimal solution. According to the offset range of approximately  $4^\circ$  to  $7^\circ$ , as mentioned in Section 1, the method searches the range  $-5 \leq \alpha \leq 5$ ,  $-5 \leq \beta \leq 5$  in degrees. In this range, the maximum offset is  $7.1^\circ$ . To improve search performance, the parameter space is divided into  $4 \times 4$  square regions, and differential evolution is applied in each region. For the final result, the parameters with minimum cost are adopted. The preceding discourse in *Fixation Detection* unequivocally demonstrates Assertion II.

## Experiments

This section demonstrates the performance of the proposed method by presenting three experiments using a common gaze dataset acquired in two VR environments. The common experimental setup is described in detail in *Experimental Setup*. In *Accuracy Evaluation*, we show the accuracy of the proposed method. *Convergence Performance* confirms the convergence performance with the walking distance. Finally, we demonstrate the effect of the accuracy of the initial parameters on the estimation accuracy in *Dependence on Initial Parameters*. All the experiments were approved by the ethics committee of the Graduate School of Engineering Science, Osaka University (R2-9) and, the participants gave informed consent.

### Experimental Setup

In this section, we explain the setup for acquiring gaze data used in the three experiments.

### ***HMD and Eye Tracker***

HTC Vive Pro Eye was used as an HMD. The resolution of the HMD is  $1440 \times 1600$  pixels per eye (total  $2880 \times 1600$  pixels), the refresh rate is 90 Hz, and the viewing angle is  $110^\circ$ . Rendering was implemented in the game engine Unity on a PC (CPU: Intel Core i7-9700K, GPU: NVIDIA GeForce RTX 2080 SUPER).

Gaze data were acquired using the HMD's built-in eye tracker with an actual acquisition rate of approximately 50 Hz. The head position and posture were acquired by the Lighthouse tracking system attached to the HMD, and the acquisition rate during the VR scene presentation was approximately 50 Hz.

We used the SRanipal SDK as a software library for acquiring gaze data. The average of the gazes of both eyes starting from the midpoint of both pupil centers obtained from this library was used as the user's gaze. In addition, using the SRanipal SDK, we can obtain the degree of eyelid opening and closing (called openness) in the range from 0.0 (completely closed) to 1.0 (wide open). To exclude blinks, we eliminated the gaze directions with the openness below 0.5.

### ***VR Environments***

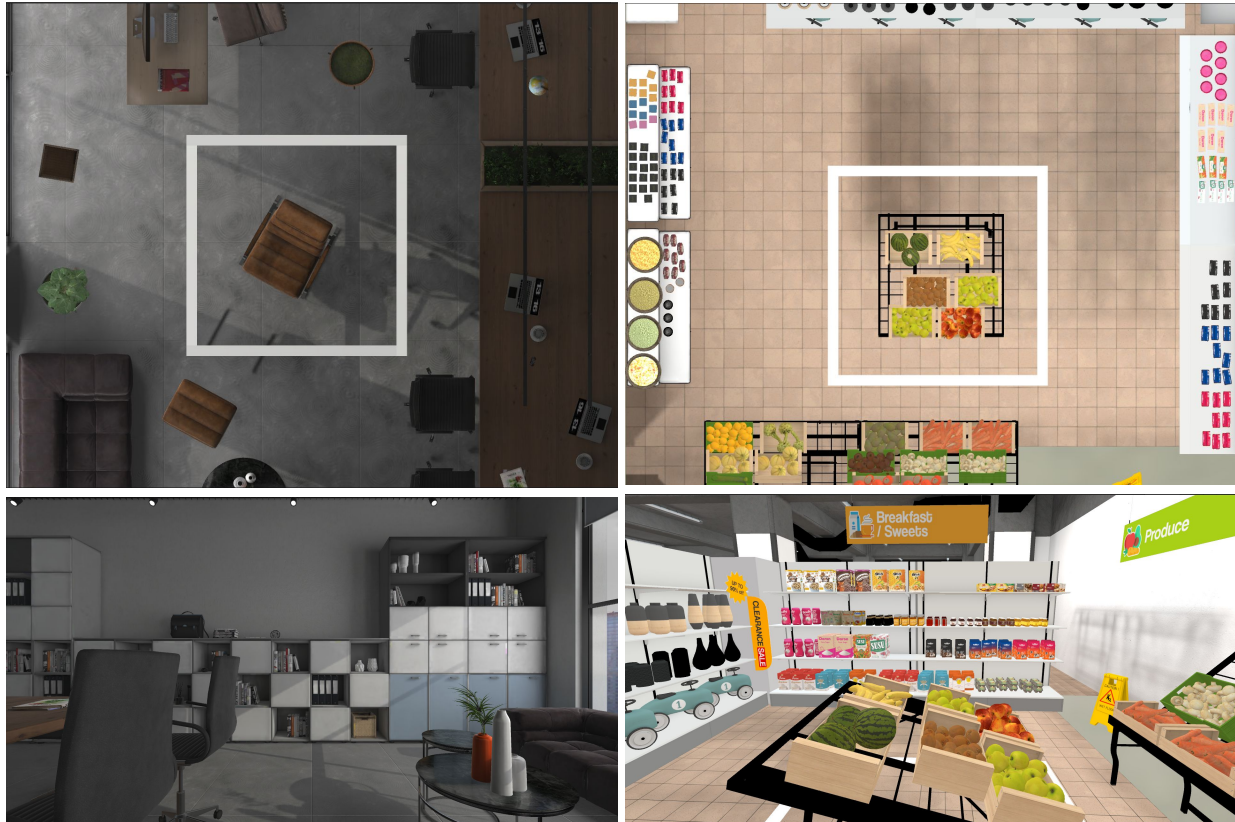
“Office Interior Archviz<sup>1</sup>” and “Modern Supermarket<sup>2</sup>,” which are available on the Unity Asset Store, were partially modified for use as VR environments. Here, they are simply named “Office” and “Supermarket,” respectively. Fig. 3 shows these two VR environments. For safety and guiding purposes, a 2 m white square outline was present on the floor, and no virtual objects were placed in the area around the white outline. The real environment was a leveled floor with no objects inside or around 1 m of the square.

### ***Participants***

Twenty-two undergraduate and graduate students with decimal visual acuity of 0.5 or better (no other visual impairment), either with naked eyes or contact lenses, participated in the

<sup>1</sup> <https://assetstore.unity.com/packages/3d/environments/urban/office-interior-archviz-155701>

<sup>2</sup> <https://assetstore.unity.com/packages/3d/environments/modern-supermarket-186122>



(a) Office

(b) Supermarket

### Figure 3

*VR environments. Each participant was asked to walk along the white outline, counterclockwise and clockwise, twice each, for a total of four consecutive laps, starting from the upper right corner.*

experiment. The mean age was 22.5 years (SD: 1.8 years). They had experience wearing some HMDs but did not understand the details of the proposed method. If, during or after the experiment, the average openness of one eye was found to be less than  $0.5^\circ$  or the average error of the control condition, described later, was found to be  $1.0^\circ$  or greater, the data of that participant were not used. As a result, gaze data were obtained for 18 participants.

### *Data Acquisition Procedure*

Gaze data were acquired while the participants were walking and freely looking around in VR environments. Each participant first received instruction on the experiments and gave

informed consent. In addition, we told the participants that they would be given some simple quizzes about the objects in the VR environments after experiencing these environments. Next, participants were asked to gaze at the markers for the traditional calibration and then walk in two different VR environments. Finally, the participant was asked to complete short quizzes about the scenes and a questionnaire about their visual acuity. These quizzes were dummy tasks. We did not use their answer data. The details of each are described below.

### ***Tasks***

To counterbalance the order effect, the participants were divided into two groups that experienced the two environments in reverse order. For each environment, starting from the upper right corner in Fig. 3, each participant was asked to walk along the white outline in the VR environments, counterclockwise and clockwise, twice each, for a total of four consecutive laps. The pace of the walk was sometimes instructed to the participant so that the total duration would be around 180 s.

### ***Thresholds for Fixation Detection***

The threshold values for each fixation detection algorithm were as follows. In I-VDT, the velocity threshold was set to  $80^\circ/\text{s}$  ( $\phi_{\text{th}} = 0.16^\circ$ ,  $S_r = 50$  Hz) and the dispersion threshold to  $0.7^\circ$  ( $D_{\text{th}} = 1.5 \times 10^{-4}$ ), following previous studies (Startsev et al., 2019) that investigated the best threshold of I-VDT by grid search. Similarly, for I-VT and I-DT, the thresholds were set to  $80^\circ/\text{s}$  and  $0.7^\circ$ , respectively. Because the minimum fixation time is generally set to a value from 100 to 200 ms (Salvucci & Goldberg, 2000), we set  $T_{\text{th}}$  to 160 ms for all three algorithms.

### ***Control Condition and Accuracy Evaluation***

We regarded the parameters estimated by traditional marker-based calibration with a 2D regression model as the control condition. The gaze direction obtained after a built-in calibration of the Vive Pro Eye for each participant was not treated as the ground truth because of its insufficient accuracy, sometimes far exceeding  $1^\circ$ . With the Vive Pro Eye, built-in calibration should be performed at least once to acquire gaze data. Therefore, the built-in calibration was performed only once for one of the authors, who is not included in the participants, and we

maintained this state while acquiring the gaze data of all the participants.

The parameters of the control condition was estimated using  $5 \times 5$  black cross markers. The markers were displayed in pseudo random order on a gray-colored plane fixed to the scene camera coordinate system and 1 m in front of the user, with a FOV angle of  $20^\circ$ . We asked each participant to gaze at each marker for 3 s. This resulted in 25 sets of gaze data for each participant. We used 16 of the these sets for the estimation of the control condition parameters; the other 9 sets were used for confirming the accuracy of the control condition and the proposed methods. Details on the methods for displaying the markers and estimating the control condition are provided in the supplemental material.

The Vive Pro Eye does not provide the optical axis, but it provides the gaze direction corresponding to the visual axis estimated by the built-in calibration process. Therefore, we generated arbitrary parameters from the control condition, i.e., the estimated visual axis. The optical axis  $\mathbf{g}_{\text{opt}}$  can be calculated from the visual axis  $\mathbf{g}_{\text{vis}}$  by the inverse transformation of Equation (2), as shown in the following equation:

$$\mathbf{g}_{\text{opt}} \propto f^{-1}(\mathbf{g}_{\text{vis}}; \boldsymbol{\theta}_{\text{offset}}). \quad (15)$$

We determined the gaze direction  $\mathbf{g}$  calibrated by arbitrary parameters  $\boldsymbol{\theta}$  by the following redefined equation:

$$\mathbf{g} \propto f^{-1}(\mathbf{g}_{\text{vis}}; \boldsymbol{\theta}). \quad (16)$$

In this case, the control condition parameters can be represented as  $\boldsymbol{\theta} = [0, 0]$ . For the evaluation of the accuracy of both the proposed method and the control condition, the estimated parameters were applied to the same nine sets, and the average absolute error from the markers was evaluated in degrees.

## Accuracy Evaluation

### *Purpose*

In this study, accuracy evaluation has two purposes. The first is to confirm the feasibility of our self-calibration method. One straightforward criterion for feasibility is that the accuracy of

the visual axis estimated by the proposed method is higher than that of the optical axis as the initial parameters obtained by the 3D eye model. The second is to determine the impact of the choice of fixation detection algorithm and the use of uncalibrated gaze data for fixation detection on accuracy.

### ***Method***

We evaluated the accuracy of the variations of the proposed method and compared the accuracy with that of the optical axis and the visual axis (control condition). As variations of the proposed method, we prepared six methods that are all possible combinations of three fixation detection algorithms (I-VT, 3D I-DT, and 3D I-VDT) and two initial values (opt: optical axis, vis: visual axis) given to each fixation detection algorithm. For all the methods, the initial parameter for optimization is the optical axis. Table 2 summarizes all the methods. For the optical axis, average offsets reported in a previous study were used. The literature (Abass et al., 2018) reported the average offsets of both eyes in a total of 1020 Brazilian, Chinese, and Italian participants. In our experiment, the offset of the cyclopean eye was approximated  $\theta_{\text{offset}} = [1.02, 3.30]$  by averaging each component of both eyes' offsets.

We applied each method to three sets of data containing fixations detected in Office, Supermarket, and their combination (named Office+Supermarket). For reference, the average absolute errors of the optical and visual axes (control condition) of all the participants were also computed. In total, the average absolute error of 20 conditions (3 detection algorithms  $\times$  2 initial values  $\times$  3 environments + 2 references) was evaluated.

For each environment condition, we performed a multiple test on the seven results of all

**Table 2**

*Combination of Fixation Detection Algorithms and Initial Parameters*

Methods	I-VT (opt)	I-VT (vis)	I-DT (opt)	I-DT (vis)	<b>I-VDT (opt)</b>	I-VDT (vis)
Fixation detection algorithms	I-VT	I-VT	I-DT	I-DT	<b>I-VDT</b>	I-VDT
Initial parameters for fixation detection	optical axis	visual axis	optical axis	visual axis	<b>optical axis</b>	visual axis
Initial parameters for optimization	optical axis	optical axis	optical axis	optical axis	<b>optical axis</b>	optical axis

the participants: the results of the six proposed methods and the optical axis. Because the prior Shapiro-Wilk test (Shapiro & Wilk, 1965) confirmed that the absolute errors of each method were not normally distributed, we applied Steel–Dwass’s method (Dwass, 1960; Steel, 1960), which is a non-parametric multiple comparison test that assumes arbitrary probability distributions.

### ***Results***

Fig. 4 shows the average absolute errors under all the conditions. First, we focus on the case “opt” and present the results of using the optical axis for fixation detection. The absolute errors of I-DT (opt) and I-VDT (opt) were significantly ( $p < 0.01$ ) lower than those of the optical axis in all environmental conditions. I-VDT (opt) in the Office + Supermarket had the highest accuracy with  $2.12^\circ$  among the “opt” methods. Meanwhile, I-VT (opt) was not significantly different from the optical axis, except in the Office.

Next, we focus on the comparison of “opt” with “vis”, i.e., the difference between the initial parameters. I-DT (vis) and I-VDT (vis) showed improved accuracy of I-DT (opt) and I-VDT (opt), respectively, under all conditions. In Office + Supermarket, I-DT (vis) and I-VDT (vis) were significantly better ( $p < 0.05$ ) for all “opt” methods. I-DT (vis) in the Office + Supermarket was the most accurate with  $1.20^\circ$ .

### ***Discussion***

Some expected results were obtained. First, the proposed method with I-VDT (opt) was more accurate than the optical axis. This means that the proposed method is applicable to gaze estimation based on the 3D eye model. None of the self-calibration methods applicable to arbitrary scenes shown in *Related Work* have been statistically shown to be more accurate in estimating calibration parameters than the optical axis. Thus, the proposed method is the first whose feasibility has been confirmed.

Second, the average absolute errors of I-VDT (opt) in any scenes were also smaller than those of any conventional self-calibration methods for arbitrary scenes (Liu et al., 2020; Murauer et al., 2018; Shi et al., 2020), i.e., about  $3^\circ$  at best. This result is consistent with the fact that scene model-based methods (Maio et al., 2011; Miki et al., 2016; Model & Eizenman, 2010a, 2010b;

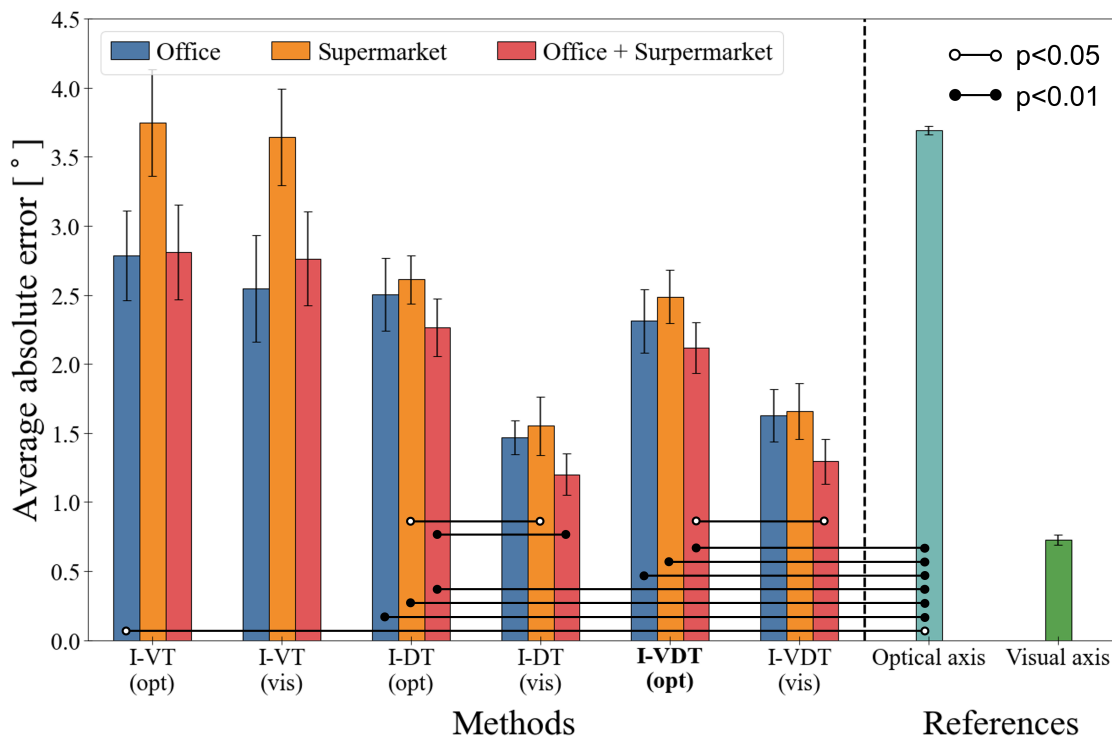


**Figure 4**

*Absolute errors of the proposed method. “opt” indicates that the initial calibration parameters corresponding to the optical axis were used in the fixation detection. Similarly, “vis” refers to fixation detection using the parameters of the visual axis. “Visual axis” represents the accuracy of the control condition with 16 of the 25 markers. “Optical axis” shows the accuracy of the optical axis generated by adding the average offset to the control condition. All the errors were evaluated with the same gaze data of the other nine markers. The error bars indicate standard errors for all participants.*

Nagamatsu, Iwamoto, et al., 2010; J. G. Wang et al., 2005) tend to be more accurate than saliency-based methods (Chen & Ji, 2015; Sugano et al., 2013) or smooth pursuit-based methods (Murauer et al., 2018), as shown in Table 1. In previous studies, participants were asked to search for a specific object (Shi et al., 2020) or to see a scene in with one salient object (Murauer et al., 2018; Tamura & Takemura, 2020) in their experiments. In our experiments, we have not employed the tasks, which could potentially increase the accuracy of the calibration. However, the statistical superiority of the proposed method cannot be determined without the unification of experimental conditions.

In contrast, unexpected results were also obtained. First, the absolute error of “vis” was smaller than that of “opt” in I-DT and I-VDT in Office + Supermarket environments. In particular, the accuracy of “vis” in I-DT was surprisingly improved to  $1.2^\circ$ , which is fairly close to the accuracy of the visual axis (green bar in Fig. 4). Note that we used the visual axis parameters only for fixation detection and not for optimization, and the effect of the different parameters on the fixation detection is only a slight increase or decrease in the number of frames judged to be fixations. This result indicates the little to no cause for inaccuracy in the optimization, and that mainly fixation detection has room for improvement. In general, calibrated gaze data must be used for fixation detection. To our knowledge, previous studies have not discussed the effect of calibration accuracy on the results of fixation detection. Therefore, in *Dependence on Initial Parameters*, we comprehensively investigate the relationship between the calibration parameters for fixation detection and the accuracy of the proposed method. The above trend did not exist in the case with I-VT. We expected this to some extent because changes in the offset of the gaze direction have little effect on the angular velocity of the gaze direction used by I-VT as a criterion. In the future, development of a fixation detection method that is less dependent on initial parameters and the optimization of parameters for the entire method including fixation detection are necessary.

Second, it was found that the accuracy of Supermarket tended to be lower and the that of Office + Supermarket tended to be higher than that of the other scenes. Although statistical

significance was not confirmed, the Office scene was more accurate than the Supermarket scene under any condition, and the same trend was observed in *Convergence Performance* and *Dependence on Initial Parameters*. The cause of this scene dependence could not be clarified in our experiments. A possible cause is the variation of surface normals. The sensitivity of the reprojection error depends on the scene distance and the surface inclination. The proposed method was expected to average out the bias owing to such sensitivity using multiple fixations because a realistic scene had surfaces with various normal directions. The abovementioned scene dependence is consistent with the results if interpreted as follows: Supermarket had a biased distribution of surface normals and was less accurate than Office; Office + Supermarket had the best accuracy owing to the enhanced averaging by the increased variations of surface normals. Another possible cause could simply be an increase in the number of fixations. This is contradicted by the experiments in the next section.

### **Convergence Performance by Walking Distance**

#### ***Purpose***

This experiment aimed to confirm the relationship between the accuracy of the estimated parameters and the cumulative translational distance of users. This relationship indicates how far the user must move to complete the calibration. The convergence speed of self-calibration is often based on time or the number of frames (Sugano et al., 2013). Because the proposed method requires fixations to occur along with the translational movement of the user's head, we confirmed the accuracy and the number of fixations with respect to the translational movement distance.

#### ***Method***

For the two VR scenes, we obtained the average absolute errors in distance intervals from 3 to 34 m in 1 m increments. A minimum distance of 3 m was considered because in some cases, fixation is not observed at distances less than 3 m. A maximum distance of 34 m was set as the shortest cumulative distance among the 18 participants. Three algorithms, I-VT, I-DT, and I-VDT, were used for fixation detection, with the optical axis as defined in *Accuracy Evaluation*. The average absolute errors at 3, 18, and 34 m were compared for the three fixation detection

algorithm. The Steel–Dwass method was used to test for differences.

### ***Results***

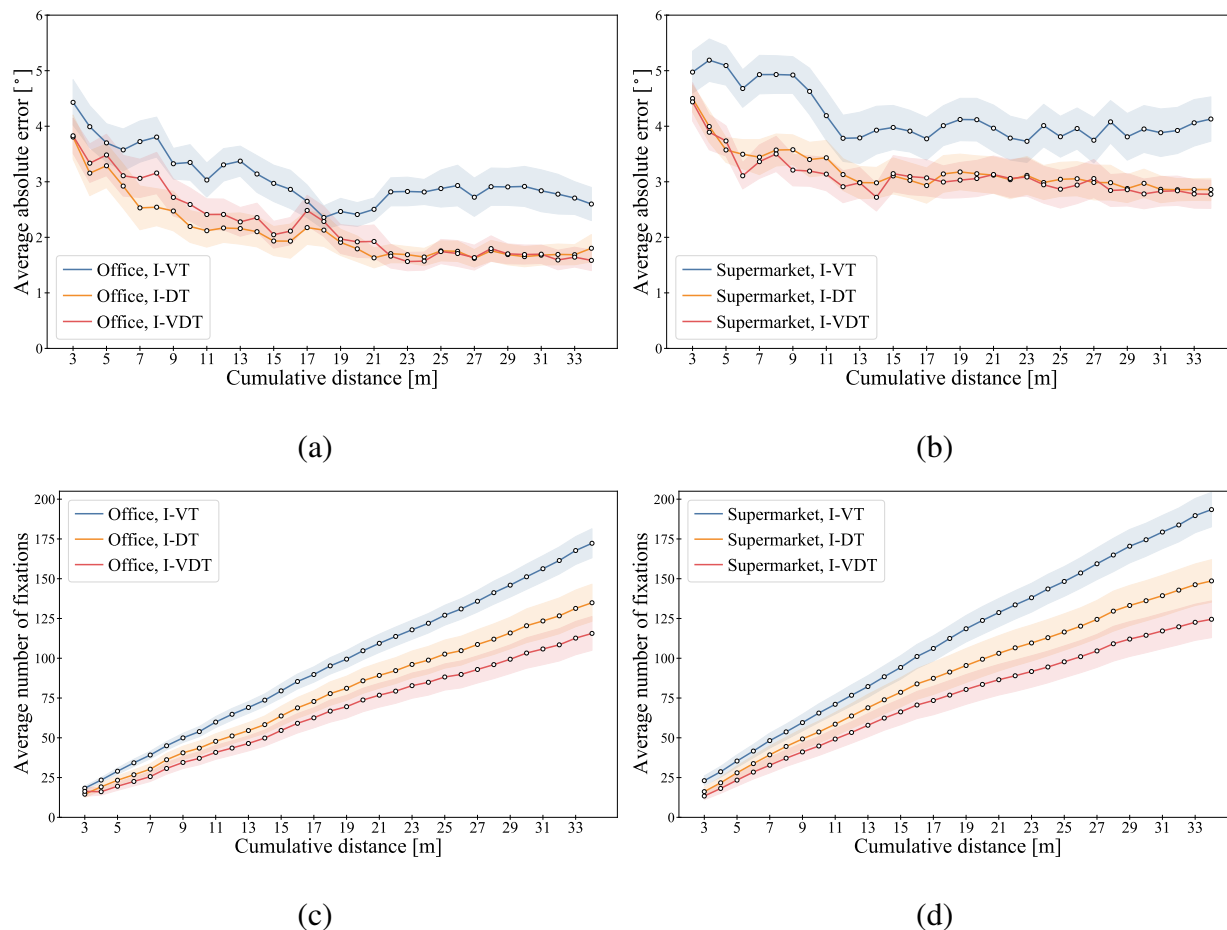
Fig. 5 (a) and (b) show the average absolute error versus cumulative distance in Office and Supermarket, respectively. Fig. 5 (c) and (d) show the average number of fixations versus cumulative distance in Office and Supermarket, respectively. The error bands with light colors along the lines indicate standard errors. Except for I-VT in Supermarket, the average errors at 18 and 34 m showed significantly higher accuracy than that at 3 m ( $p < 0.05$ ). No significant difference was found between the average errors at 18 and 34 m. I-VT in Supermarket showed no significant difference between any two of the three distances.

The number of fixations decreased in the order of I-VT, I-DT, and I-VDT at any distance. Significant differences between I-VT and I-VDT were confirmed at 3 ( $p < 0.05$ ), 18 ( $p < 0.05$ ), and 34 m ( $p < 0.01$ ). For reference, the average computation times of the two scenes were 10, 28, and 56 s at 3, 18, and 34 m, respectively, in the case of I-VDT.

### ***Discussion***

The accuracy of the proposed method in I-DT and I-VDT improved significantly at the cumulative distance of 18 m compared with that at the start of walking, and this value is not significantly different from the accuracy at 34 m. Therefore, the parameters almost converge after a walking distance of about 20 m. The speed to reach 34 m in 180 s is approximately 0.7 km/h, which is considerably slower than the typical walking speed of 4 km/h. This is because we could only prepare a small environment, and we instructed them to walk at such a speed. Considering that the proposed method utilizes the translation of the head position, even faster convergence can possibly be achieved if the user walks at normal speed.

Although the trend was for the error to decrease with distance, at some distances, the error locally increased in both scenes even with I-DT and I-VDT. We present four possible hypotheses regarding the cause of this increase: (i) the head position was almost stationary, (ii) few fixations were detected, (iii) the dispersion of the detected fixations was large, and (iv) the inclination of the surface where the PoRs of fixations are distributed was biased. According to Hypothesis (i),

**Figure 5**

*Absolute error and number of fixations. The cumulative distance is the sum of the translational distances of the scene cameras between adjacent frames.*

fixations detected without head movement adversely affect parameter estimation. However, in that case, the number of fixations at that distance should rapidly increase because the cumulative distance does not increase. As shown in Fig. 5 (c) and (b), no such increase is found; thus, Hypothesis (i) does not hold. In contrast, if no fixation is detected as the cumulative distance increases, the absolute error should remain constant. Therefore, Hypothesis (ii) is also rejected because the same is true. Hypothesis (iii) cannot be ruled out because the dispersion of the fixation depends on psychological states (Hafed & Clark, 2002). We asked each participant to pace themselves or reverse their walking direction, which may have led to a loss of concentration. In our method, such psychological factors are not taken into account. Regarding Hypothesis (iv),

the possibility of a bias in the inclination of the surface at some distances cannot be ruled out.

## Dependence on Initial Parameters

### *Purpose*

This experiment was performed to analyze the dependence of the accuracy of the proposed method on the initial calibration parameters used for fixation detection. As mentioned in *Related Work*, in general, fixation detection results depend on the algorithm and the initial calibration parameters. To the best of our knowledge, there is no study on fixation detection using uncalibrated parameters. In this section, we confirm the effect of the initial parameters of fixation detection on the accuracy of the proposed method.

### *Method*

The parameter space was divided into five regions, and each region was referred to as Range 1–5. We define Range  $l$  as  $l - 1 \leq |\alpha| \leq l$  or  $l - 1 \leq |\beta| \leq l$  ( $l = 1, 2, \dots, 5$  in degrees). Fifty sets of random calibration parameters  $[\alpha, \beta]$  were generated with the uniform distribution for each parameter range, and fixation detection was performed using each set of parameters. We obtained the calibration accuracy for each participant using the fixation detection results and computed the average absolute error for each parameter range. Consequently, we acquired 900 results ( $= 50$  parameters  $\times$  18 participants). The same accuracy results were obtained for six conditions: two scenes (Office, Supermarket) and three algorithms (I-VT, I-DT, I-VDT). As in the experiments described above, the Steel–Dwass method was applied for testing against a set of parameter ranges for each condition.

### *Results*

Fig. 6 shows the relationship between calibration accuracy and parameter range. The error bands with light colors along the lines indicate standard errors. In the cases of I-DT and I-VDT, any two of the parameter ranges were significantly different ( $p < 0.01$ ) from each other in both scenes. For I-VT in Office, significant differences ( $p < 0.01$ ) were observed between Range 1 and any of Range 3–5 and between Range 2 and any of Range 4 and 5. For I-VT in Supermarket, no

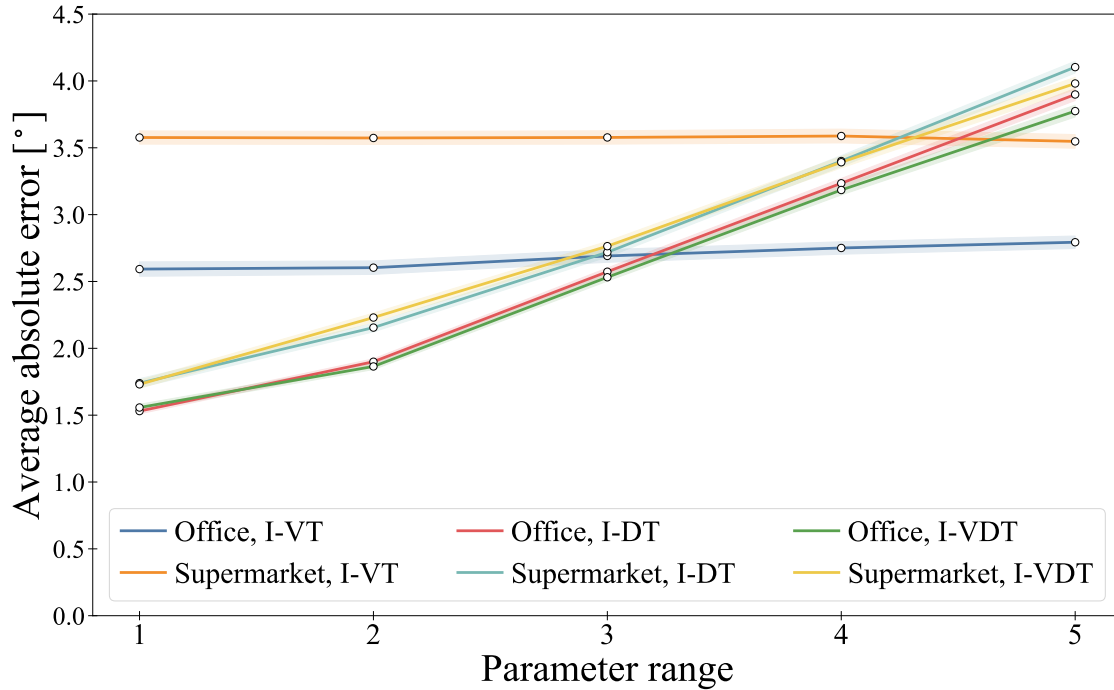


**Figure 6**

*Dependence on parameters for fixation detection. Range  $l$  indicates  $l - 1 \leq |\alpha| \leq l$  or  $l - 1 \leq |\beta| \leq l$  ( $l = 1, 2, \dots, 5$  in degrees). The bands with light colors indicate standard errors.*

significant difference was observed between any two parameter ranges.

In Office, the absolute error of the three methods was comparable in Range 3. In Supermarket, the absolute error of I-VT, I-DT, and I-VDT were comparable in Range 4. Therefore, I-DT and I-VDT are superior for Range 1 and 2, whereas I-VT is superior for Range 5. In addition to the results of the accuracy evaluation shown in Fig. 4, the absolute error was lower in Supermarket than in Office for all parameter ranges of any of the fixation detection algorithms.

### ***Discussion***

Fig. 6 clearly shows that some fixation detection algorithms such as I-VT have almost no parameter dependence on accuracy and that the initial calibration parameters for fixation detection with I-DT and I-VDT have a strong influence on the overall processing. The fact that accurate initial parameters are needed to estimate accurate calibration parameters may seem to be a “chicken-or-egg” situation; nevertheless, the proposed method was able to estimate parameters

with higher accuracy than the optical axis. To further improve accuracy, two issues need to be addressed: providing accurate initial parameters and developing an accurate fixation detection method with lower parameter dependence.

The output of the conventional methods can be used to obtain accurate initial parameters. For accurate fixation detection methods, fortunately, our experiments allow a quantitative evaluation of the accuracy of a fixation detection method itself. Studies on the objective and quantitative evaluation of fixation detection methods are limited and do not deal with 3D scenes where the head moves (Blignaut, 2009; Komogortsev & Karpov, 2013).

In summary, based on the preceding results, it becomes apparent that Assertion III has been elucidated.

### **Limitations**

It has been demonstrated that by showing Assertions I to III, the proposed method can automatically calibrate an eye-tracker with an accuracy approximately  $2^\circ$  in a situation where the head moves within arbitrary 3D environment without using images. In this section, we clarify the limitations of the proposed method.

### **Statistical Comparison with Previous Studies**

The qualitative comparisons in Table 1 show that the conventional methods available for 3D environments (Liu et al., 2020; Murauer et al., 2018; Shi et al., 2020; Tamura & Takemura, 2020) are directly comparable to the proposed method. However, we did not perform a quantitative comparison with these conventional methods. The same is true of most of studies on these conventional methods. The reason is probably the same as ours: the source code is not open, and implementation details are not sufficiently clear. Therefore, the standardization of evaluation methods and quantitative comparison under the same conditions will be our focus in future work.

### **Moving & Deforming Objects**

To avoid complications in implementation, we did not include moving objects in the VR scenes. A smooth pursuit to gaze at a moving object is equivalent to a moving head in the object coordinate system. Theoretically, the presence of moving objects should work to the advantage of

our method.

Moving or deforming objects complicate the calculation of the collision position in the gaze direction. In particular, the collision point depends on the time as well as the position and orientation of the scene camera. Therefore, during optimization, the collision points must be calculated with various parameters at various times. The implementation can be simplified using only the line of sight to static objects.

### **Physiological & Psychological Factors**

The proposed method does not take optokinetic response (OKR) and vestibulo-ocular reflex (VOR) into account, although free head movement and rotation are assumed. The accuracy of the proposed method could be improved using a mathematical model of OKR or VOR gain, which causes gaze shift. In addition, the proposed method does not take psychological effects into account. The introduction of oculomotor and psychological models is a future challenge.

### **Cyclopean Eye**

In many conventional scene model-based methods, both eyes are treated independently. In contrast, in this study, we applied the scene camera at the cyclopean eye, as mentioned in *Discussion of Accuracy Evaluation*, because independently treating both eyes was expected to have little effect. The scene depth in our experimental environments was dominated by the region over 5 m, and we expected that the change in convergence angle would not be stable compared with the case of a planar monitor placed at about 1 m. Because many gaze analyses use some method of averaging the gaze directions of both eyes (Nakamura & Shimojo, 2003; H. Wang et al., 2018), we conclude that the proposed method is at least effective for such applications.

### **Optimization Algorithm & Computation Time**

Many local solutions to the optimization of the proposed method are available. Differential evolution is less accurate than the brute force method. The calculation of collision points and the projection of PoRs require most of the computation time during optimization, which can be parallelized. Therefore, there is room for improving the computation time.

## **AR Scenario**

The proposed method is suitable for VR environments because of its assumptions about scene models and head postures; theoretically, it can be also extended to AR environments. The difference between AR and VR is the accuracy of the scene model. The effects of the scene model and head pose accuracy on calibration accuracy is a topic of great importance and interest.

## **Conclusion**

In this study, we propose a self-calibration method for an eye-tracking VR HMD based on fixation detection. Although the proposed method can be categorized as a scene model-based method, it is applicable to arbitrary scenes with large head movements and a large number of occlusions, unlike conventional methods. The proposed method can automatically calibrate the eye tracker with an accuracy of about  $2^\circ$  in about 30 s if the user walks about 20 m. The 3D I-VDT algorithm is the best for fixation detection in terms of accuracy and computational cost compared with the I-VT and 3D I-DT algorithm. The evaluation function for optimization has little room for improvement. Further improvement in accuracy can be achieved by developing a fixation detection algorithm that is less dependent on the initial calibration accuracy or by developing a method for the simultaneous optimization of both the calibration parameters and the fixation detection results. Quantitative comparison with conventional methods under uniform conditions is the main future research avenue.

## **Acknowledgments**

This work was supported in part by the JSPS Grant-in-Aid for Scientific Research No. 21K03964 and 22H03632.

### References

- Abass, A., Vinciguerra, R., Lopes, B. T., Bao, F., Vinciguerra, P., Ambrósio, R., Jr., & Elsheikh, A. (2018). Positions of ocular geometrical and visual axes in Brazilian, Chinese and Italian populations. *Current Eye Research, 43*(11), 1404–1414.  
<https://doi.org/10.1080/02713683.2018.1500609>
- Akinyelu, A. A., & Blignaut, P. (2020). Convolutional neural network-based methods for eye gaze estimation: A survey. *IEEE Access, 8*, 142581–142605.  
<https://doi.org/10.1109/ACCESS.2020.3013540>
- Alnajjar, F., Gevers, T., Valenti, R., & Ghebreab, S. (2017). Auto-calibrated gaze estimation using human gaze patterns. *International Journal of Computer Vision, 124*(2), 223–236.  
<https://doi.org/https://doi.org/10.1007/s11263-017-1014-x>
- Baluja, S., & Pomerleau, D. A. (1993). Non-intrusive gaze tracking using artificial neural networks. *Proceedings of the 6th International Conference on Neural Information Processing Systems, 753–760*.
- Beymer, D., & Flickner, M. (2003). Eye gaze tracking using an active stereo head. *Proceedings of the 2003 IEEE Computer Society Conference on Computer Vision and Pattern Recognition, 2*, 451–458. <https://doi.org/10.1109/CVPR.2003.1211502>
- Blignaut, P. (2009). Fixation identification: The optimum threshold for a dispersion algorithm. *Attention, Perception & Psychophysics, 71*, 881–895.  
<https://doi.org/https://doi.org/10.3758/APP.71.4.881>
- Blignaut, P. (2013). Mapping the pupil-glint vector to gaze coordinates in a simple video-based eye tracker. *Journal of Eye Movement Research, 7*(1), 1–11.  
<https://doi.org/10.16910/jemr.7.1.4>
- Carpenter, R. H. S. (1988). *Movements of the eyes*. Pion.
- Chen, J., & Ji, Q. (2011). Probabilistic gaze estimation without active personal calibration. *Proceedings of the 2011 IEEE Conference on Computer Vision and Pattern Recognition, 609–616*. <https://doi.org/10.1109/CVPR.2011.5995675>

- Chen, J., & Ji, Q. (2015). A probabilistic approach to online eye gaze tracking without explicit personal calibration. *IEEE Transactions on Image Processing*, 24(3), 1076–1086.  
<https://doi.org/10.1109/TIP.2014.2383326>
- Dwass, M. (1960). Some k-sample rank-order tests. In *Contributions to probability and statistics* (pp. 198–202).
- Guestrin, E. D., & Eizenman, M. (2006). General theory of remote gaze estimation using the pupil center and corneal reflections. *IEEE Transactions on Biomedical Engineering*, 53(6), 1124–1133. <https://doi.org/10.1109/TBME.2005.863952>
- Hafed, Z. M., & Clark, J. J. (2002). Microsaccades as an overt measure of covert attention shifts. *Vision Research*, 42(22), 2533–2545.  
[https://doi.org/https://doi.org/10.1016/S0042-6989\(02\)00263-8](https://doi.org/https://doi.org/10.1016/S0042-6989(02)00263-8)
- Hansen, D. W., Hansen, J. P., Nielsen, M., Johansen, A. S., & Stegmann, M. B. (2002). Eye typing using Markov and active appearance models. *Proceedings of the Sixth IEEE Workshop on Applications of Computer Vision*, 132–136. <https://doi.org/10.1109/ACV.2002.1182170>
- Hansen, D. W., & Ji, Q. (2010). In the eye of the beholder: A survey of models for eyes and gaze. *IEEE Transactions on Pattern Analysis and Machine Intelligence*, 32(3), 478–500.  
<https://doi.org/10.1109/TPAMI.2009.30>
- Hessels, R. S., Niehorster, D. C., Nyström, M., Andersson, R., & Hooge, I. T. C. (2018). Is the eye-movement field confused about fixations and saccades? a survey among 124 researchers. *Royal Society Open Science*, 5(8), 1–23.  
<https://doi.org/https://doi.org/10.1098/rsos.180502>
- Hiroe, M., Mitsunaga, S., & Nagamatsu, T. (2019). Implicit user calibration for model-based gaze-tracking system using face detection around optical axis of eye. *Proceedings of the Extended Abstracts of the 2019 CHI Conference on Human Factors in Computing Systems*. <https://doi.org/10.1145/3290607.3312942>

- Hooge, I. T. C., Niehorster, D. C., Nyström, M., Andersson, R., & Hessels, R. S. (2022). Fixation classification: How to merge and select fixation candidates. *Behavior Research Methods*, *54*(6), 2765–2776. <https://doi.org/10.3758/s13428-021-01723-1>
- Hu, Z., Li, S., Zhang, C., Yi, K., Wang, G., & Manocha, D. (2020). DGaze: CNN-based gaze prediction in dynamic scenes. *IEEE Transactions on Visualization and Computer Graphics*, *26*(5), 1902–1911. <https://doi.org/10.1109/TVCG.2020.2973473>
- Hu, Z., Zhang, C., Li, S., Wang, G., & Manocha, D. (2019). SGaze: A data-driven eye-head coordination model for realtime gaze prediction. *IEEE Transactions on Visualization and Computer Graphics*, *25*(5), 2002–2010. <https://doi.org/10.1109/TVCG.2019.2899187>
- Jurado, J. L., Morales, J. M., Guixeres, J., & Alcañiz, M. (2020). Development and calibration of an eye-tracking fixation identification algorithm for immersive virtual reality. *Sensors*, *20*(17), 1–15. <https://doi.org/10.3390/s20174956>
- Kar, A., & Corcoran, P. (2017). A review and analysis of eye-gaze estimation systems, algorithms and performance evaluation methods in consumer platforms. *IEEE Access*, *5*, 16495–16519. <https://doi.org/10.1109/ACCESS.2017.2735633>
- Komogortsev, O. V., & Karpov, A. (2013). Automated classification and scoring of smooth pursuit eye movements in the presence of fixations and saccades. *Behavior research methods*, *45*(1), 203–215. <https://doi.org/https://doi.org/10.3758/s13428-012-0234-9>
- Konrad, R., Angelopoulos, A., & Wetzstein, G. (2020). Gaze-contingent ocular parallax rendering for virtual reality. *ACM Transactions on Graphics*, *39*(2), 1–12. <https://doi.org/https://doi.org/10.1145/3361330>
- Krafka, K., Khosla, A., Kellnhofer, P., Kannan, H., Bhandarkar, S., Matusik, W., & Torralba, A. (2016). Eye tracking for everyone. *Proceedings of the 2016 IEEE Conference on Computer Vision and Pattern Recognition*, 2176–2184. <https://doi.org/10.1109/CVPR.2016.239>

- Krajancich, B., Kellnhofer, P., & Wetzstein, G. (2020). Optimizing depth perception in virtual and augmented reality through gaze-contingent stereo rendering. *ACM Transactions on Graphics*, 39(6), 1–10. <https://doi.org/10.1145/3414685.3417820>
- Larsson, L., Schwaller, A., Nyström, M., & Stridh, M. (2016). Head movement compensation and multi-modal event detection in eye-tracking data for unconstrained head movements. *Journal of Neuroscience Methods*, 274, 13–26. <https://doi.org/10.1016/j.jneumeth.2016.09.005>
- Li, Y., Fathi, A., & Rehg, J. M. (2013). Learning to predict gaze in egocentric video. *Proceedings of the 2013 IEEE International Conference on Computer Vision*, 3216–3223. <https://doi.org/10.1109/ICCV.2013.399>
- Liu, M., Li, Y., & Liu, H. (2020). 3D gaze estimation for head-mounted eye tracking system with auto-calibration method. *IEEE Access*, 8, 104207–104215. <https://doi.org/10.1109/ACCESS.2020.2999633>
- Maior, W., Chen, J., & Ji, Q. (2011). Constraint-based gaze estimation without active calibration. *Proceedings of the IEEE International Conference on Automatic Face & Gesture Recognition*, 627–631. <https://doi.org/10.1109/FG.2011.5771469>
- Manor, B. R., & Gordon, E. (2003). Defining the temporal threshold for ocular fixation in free-viewing visuocognitive tasks. *Journal of Neuroscience Methods*, 128(1), 85–93. [https://doi.org/10.1016/s0165-0270\(03\)00151-1](https://doi.org/10.1016/s0165-0270(03)00151-1)
- Mardanbegi, D., Langlotz, T., & Gellersen, H. (2019). Resolving target ambiguity in 3D gaze interaction through VOR depth estimation. *Proceedings of the 2019 CHI Conference on Human Factors in Computing Systems*. <https://doi.org/https://doi.org/10.1145/3290605.3300842>
- Massé, B., Ba, S., & Horaud, R. (2018). Tracking gaze and visual focus of attention of people involved in social interaction. *IEEE Transactions on Pattern Analysis and Machine Intelligence*, 40(11), 2711–2724. <https://doi.org/10.1109/TPAMI.2017.2782819>

- Meng, X., Du, R., Zwicker, M., & Varshney, A. (2018). Kernel foveated rendering. *Proceedings of the ACM on Computer Graphics and Interactive Techniques*, 1(1), 1–20.  
<https://doi.org/https://doi.org/10.1145/3203199>
- Miki, K., Nagamatsu, T., & Hansen, D. W. (2016). Implicit user calibration for gaze-tracking systems using kernel density estimation. *Proceedings of the Ninth Biennial ACM Symposium on Eye Tracking Research & Applications*, 249–252.  
<https://doi.org/https://doi.org/10.1145/2857491.2857518>
- Model, D., & Eizenman, M. (2010a). An automatic personal calibration procedure for advanced gaze estimation systems. *IEEE Transactions on Biomedical Engineering*, 57(5), 1031–1039. <https://doi.org/10.1109/TBME.2009.2039351>
- Model, D., & Eizenman, M. (2010b). User-calibration-free remote gaze estimation system. *Proceedings of the 2010 Symposium on Eye-Tracking Research & Applications*, 1–8.  
<https://doi.org/10.1145/1743666.1743672>
- Murauer, M., Haslgrübler, M., & Ferscha, A. (2018). Natural pursuits for eye tracker calibration. *Proceedings of the 5th international Workshop on Sensor-based Activity Recognition and Interaction*. <https://doi.org/https://doi.org/10.1145/3266157.3266207>
- Nagamatsu, T., Hiroe, M., & Arai, H. (2021). Extending the measurement angle of a gaze estimation method using an eye model expressed by a revolution about the optical axis of the eye. *IEICE Transactions on Information and Systems*, E104.D(5), 729–740.  
<https://doi.org/10.1587/transinf.2020EDP7072>
- Nagamatsu, T., Iwamoto, Y., Kamahara, J., Tanaka, N., & Yamamoto, M. (2010). Gaze estimation method based on an aspherical model of the cornea: Surface of revolution about the optical axis of the eye. *Proceedings of the 2010 Symposium on Eye-Tracking Research & Applications*, 255–258. <https://doi.org/https://doi.org/10.1145/1743666.1743726>
- Nagamatsu, T., Kamahara, J., Iko, T., & Tanaka, N. (2008). One-point calibration gaze tracking based on eyeball kinematics using stereo cameras. *Proceedings of the 2008 Symposium on*

- Eye Tracking Research & Applications*, 95–98.  
<https://doi.org/https://doi.org/10.1145/1344471.1344496>
- Nagamatsu, T., Sugano, R., Iwamoto, Y., Kamahara, J., & Tanaka, N. (2010). User-calibration-free gaze tracking with estimation of the horizontal angles between the visual and the optical axes of both eyes. *Proceedings of the 2010 Symposium on Eye-Tracking Research & Applications*, 251–254.  
<https://doi.org/https://doi.org/10.1145/1743666.1743725>
- Nagamatsu, T., Ueki, T., & Kamahara, J. (2013). Automatic user calibration for gaze-tracking systems by looking into the distance. *Proceedings of the 3rd International Workshop on Pervasive Eye Tracking and Mobile Eye-Based Interaction*.
- Nakamura, S., & Shimojo, S. (2003). Sustained deviation of gaze direction can affect “inverted vection” induced by the foreground motion. *Vision Research*, 43(7), 745–749.  
[https://doi.org/https://doi.org/10.1016/S0042-6989\(03\)00081-6](https://doi.org/https://doi.org/10.1016/S0042-6989(03)00081-6)
- Orisaka, T., & Okatani, T. (2016). A gaze-reactive display for simulating depth-of-field of eyes when viewing scenes with multiple depths. *IEICE Transactions on Information and Systems*, E99.D(3), 739–746. <https://doi.org/10.1587/transinf.2015edp7110>
- Padmanaban, N., Konrad, R., & Wetzstein, G. (2019). Autofocals: Evaluating gaze-contingent eyeglasses for presbyopes. *Science Advances*, 5(6), eaav6187.  
<https://doi.org/10.1126/sciadv.aav618>
- Poole, A., & Ball, L. J. (2006). Eye tracking in human-computer interaction and usability research: Current status and future prospects. *Proceedings of the Encyclopedia of Human Computer Interaction*, 211–219.
- Salvucci, D. D., & Goldberg, J. H. (2000). Identifying fixations and saccades in eye-tracking protocols. *Proceedings of the 2000 Symposium on Eye Tracking Research & Applications*, 71–78. <https://doi.org/https://doi.org/10.1145/355017.355028>
- Shapiro, S. S., & Wilk, M. B. (1965). An analysis of variance test for normality (complete samples). *Biometrika*, 52(3-4), 591–611.

- Shi, P., Billeter, M., & Eisemann, E. (2020). SalientGaze: Saliency-based gaze correction in virtual reality. *Computers & Graphics, 91*, 83–94.  
<https://doi.org/https://doi.org/10.1016/j.cag.2020.06.007>
- Shic, F., Scassellati, B., & Chawarska, K. (2008). The incomplete fixation measure. *Proceedings of the 2008 Symposium on Eye Tracking Research & Applications*, 111–114.  
<https://doi.org/10.1145/1344471.1344500>
- Stampe, D. M. (1993). Heuristic filtering and reliable calibration methods for video-based pupil-tracking systems. *Behavior Research Methods, Instruments, & Computers, 25*(2), 137–142.
- Startsev, M., Agtzidis, I., & Dorr, M. (2019). 1d CNN with BLSTM for automated classification of fixations. *Behavior Research Methods, 51*(2), 556–572.  
<https://doi.org/10.3758/s13428-018-1144-2>
- Steel, R. G. D. (1960). A rank sum test for comparing all pairs of treatments. *Technometrics, 2*(2), 197–207.
- Steil, J., Huang, M. X., & Bulling, A. (2018). Fixation detection for head-mounted eye tracking based on visual similarity of gaze targets. *Proceedings of the 2018 ACM Symposium on Eye Tracking Research & Applications*.  
<https://doi.org/https://doi.org/10.1145/3204493.3204538>
- Stiefelhagen, R., Yang, J., & Waibel, A. (1997). Tracking eyes and monitoring eye gaze. *Proceedings of the Workshop on Perceptual User Interfaces*, 98–100.
- Storn, R., & Price, K. (1997). Differential evolution – A simple and efficient heuristic for global optimization over continuous spaces. *Journal of Global Optimization, 11*(4), 341–359.
- Su, S., Gu, S., Zhao, Y., Chen, Z., Wang, H., & Yang, W. (2020). Human-ocular-physiological-characteristics- based adaptive console design. *IEEE Access, 8*, 109596–109607. <https://doi.org/10.1109/ACCESS.2020.3002543>

- Sugano, Y., Matsushita, Y., & Sato, Y. (2013). Appearance-based gaze estimation using visual saliency. *IEEE Transactions on Pattern Analysis and Machine Intelligence*, 35(2), 329–341. <https://doi.org/10.1109/TPAMI.2012.101>
- Tamura, Y., & Takemura, K. (2020). Estimating point-of-gaze using smooth pursuit eye movements without implicit and explicit user-calibration. *Proceedings of the ACM Symposium on Eye Tracking Research & Applications*. <https://doi.org/https://doi.org/10.1145/3379156.3391343>
- Tan, K. H., Kriegman, D. J., & Ahuja, N. (2002). Appearance-based eye gaze estimation. *Proceedings of 6-th IEEE Workshop on Applications of Computer Vision*, 191–195. <https://doi.org/10.1109/ACV.2002.1182180>
- Uramune, R., Ikeda, S., Ishizuka, H., & Oshiro, O. (2021). Automatic calibration of eye trackers using 3D positions of fixations and virtual object surface shapes [(in Japanese)]. *IPSJ SIG Technical Report, 2021-CVIM-224*.
- Velloso, E., Wirth, M., Weichel, C., Esteves, A., & Gellersen, H. (2016). AmbiGaze: Direct control of ambient devices by gaze. *Proceedings of the 2016 ACM Conference on Designing Interactive Systems*. <https://doi.org/10.1145/2901790.2901867>
- Villanueva, A., Cabeza, R., & Porta, S. (2007). Gaze tracking system model based on physical parameters. *International Journal of Pattern Recognition and Artificial Intelligence*, 21(5), 855–877. <https://doi.org/https://doi.org/10.1142/S0218001407005697>
- Wang, H., Pi, J., Qin, T., Shen, S., & Shi, B. E. (2018). SLAM-based localization of 3D gaze using a mobile eye tracker. *Proceedings of the 2018 ACM Symposium on Eye Tracking Research & Applications*. <https://doi.org/10.1145/3204493.3204584>
- Wang, J. G., Sung, E., & Venkateswarlu, R. (2005). Estimating the eye gaze from one eye. *Computer Vision and Image Understanding*, 98(1), 83–103. <https://doi.org/https://doi.org/10.1016/j.cviu.2004.07.008>
- Wang, K., & Ji, Q. (2018). 3D gaze estimation without explicit personal calibration. *Pattern Recognition*, 79, 216–227. <https://doi.org/https://doi.org/10.1016/j.patcog.2018.01.031>

- Wang, K., Wang, S., & Ji, Q. (2016). Deep eye fixation map learning for calibration-free eye gaze tracking. *Proceedings of the Ninth Biennial ACM Symposium on Eye Tracking Research & Applications*, 47–55. <https://doi.org/10.1145/2857491.2857515>
- Wang, S., Wang, J., Peng, H., Gao, S., & He, D. (2016). A new calibration-free gaze tracking algorithm based on DE-SLFA. *Proceedings of the 2016 8th International Conference on Information Technology in Medicine and Education*, 380–384. <https://doi.org/10.1109/ITME.2016.0091>
- White, K. P., Hutchinson, T. E., & Carley, J. M. (1993). Spatially dynamic calibration of an eye-tracking system. *IEEE Transactions on Systems, Man, and Cybernetics*, 23(4), 1162–1168. <https://doi.org/10.1109/21.247897>
- Williams, O., Blake, A., & Cipolla, R. (2006). Sparse and semi-supervised visual mapping with the S<sup>3</sup>GP. *Proceedings of the 2006 IEEE Computer Society Conference on Computer Vision and Pattern Recognition*, 1, 230–237. <https://doi.org/10.1109/CVPR.2006.285>
- Xu, L. Q., Machin, D., & Sheppard, P. (1998). A novel approach to real-time non-intrusive gaze finding. *Proceedings of the British Machine Conference*, 428–437. <https://doi.org/10.5244/C.12.43>
- Zhang, X., Sugano, Y., Fritz, M., & Bulling, A. (2015). Appearance-based gaze estimation in the wild. *Proceedings of the IEEE Conference on Computer Vision and Pattern Recognition*, 4511–4520. <https://doi.org/10.1109/CVPR.2015.7299081>
- Zhu, Z., & Ji, Q. (2004). Eye and gaze tracking for interactive graphic display. *Machine Vision and Applications*, 15(3), 79–85. <https://doi.org/10.1145/569005.569017>
- Zhu, Z., Ji, Q., & Bennett, K. P. (2006). Nonlinear eye gaze mapping function estimation via support vector regression. *Proceedings of the 18th International Conference on Pattern Recognition*, 1132–1135. <https://doi.org/10.1109/ICPR.2006.864>

## Appendix

### Calibration Process

#### Implementation Details

In our manuscript, three different calibration methods are referred to, which may confuse readers. We have summarized the relationship between these calibration methods as a schematic in Fig A1. In this section, we explain the differences between and the necessity of these calibration methods.

The first involves the use of the built-in calibration tool of the HTC Vive Pro Eye. The important point is that, whatever its accuracy, any data cannot be obtained without performing this calibration process. To overcome this limitation, one of the authors performed this calibration before data acquisition from the participants of our experiments. Another point is that this eye tracker provides only the visual axis calibrated by this process and not the optical axis. Unfortunately, the accuracy of this visual axis was low, often exceeding  $1^\circ$ . Therefore, the second calibration method described below is required.

The second calibration method is applied to compensate for the lack of accuracy of the calibration tool. This method is referred to as traditional calibration or traditional marker-based calibration in our manuscript and is mainly described in this document. In this method, a well-known regression model and a sufficient number of markers are used to accurately estimate the visual axis. We detail this method in the next section and in *Calibration Error*.

The third calibration method is the self-calibration method proposed in our study. It employs a 3D eye model and computes the approximate optical axis  $\mathbf{g}_{\text{opt}}$  at the typical offset angles and the gaze direction  $\mathbf{g}$  corresponding to the arbitrary parameters for optimization based on the reliable visual axis estimated in the second calibration. This is discussed in detail in *Control Condition and Accuracy Evaluation* in our manuscript, and is therefore omitted from this document.

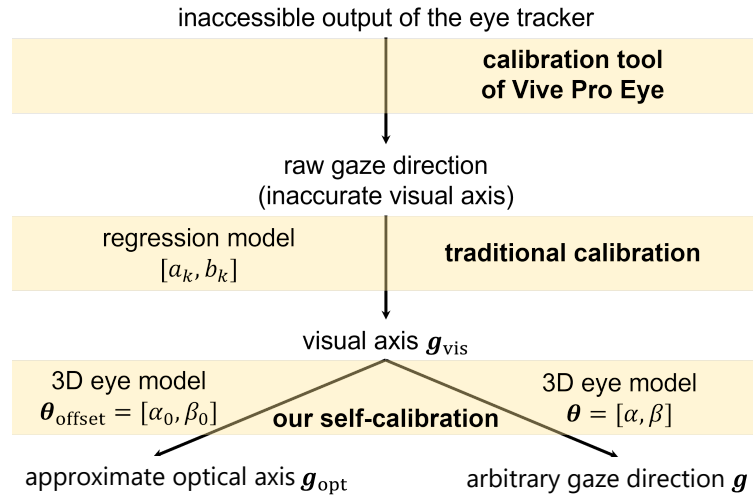


**Figure A1**

*Schematic of the calibration process in our experiment. Three types of calibration method are used in this process. This document describes the traditional calibration method for estimating the visual axis.*

### Setup of Calibration Markers

This section details the experimental setup for the traditional calibration. In particular, we explain the relationship between the scene camera that represents the user's field of view (FOV), marker positions, and eye positions. We also describe the arrangement of two types of markers: one for estimation and the other for evaluation.

We used  $5 \times 5$  black cross markers. The markers were displayed one by one in pseudo random order on a gray-colored plane fixed in the scene camera coordinate system 1 m in front of the user, with a FOV angle of  $20^\circ$  both horizontally and vertically. Fig. A2 shows the positional relationship between the scene camera, markers, and both eyes. Our method requires two kinds of pinhole scene cameras: a single camera for gaze analysis and stereoscopic cameras for rendering. We created the scene camera for analysis by translating one of the cameras for rendering. The origin of the scene camera was placed at the midpoint of both pupil centers obtained by the eye tracker. The pose was set to the same as those of the cameras for rendering, which were at the

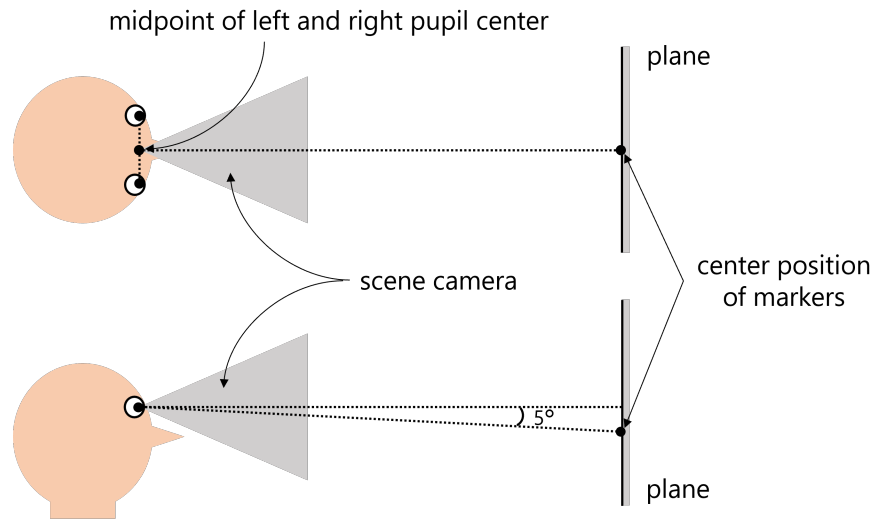


**Figure A2**

*Relationship between the scene camera, marker positions, and eye positions. The scene camera was placed at the center of both eyes. The center of markers was positioned vertically downward from the  $z$ -axis of the scene camera by approximately  $5^\circ$ .*

default setting obtained by the Lighthouse tracking system attached to the head-mounted device. Because the vertical FOV of humans is approximately  $10^\circ$ – $20^\circ$  wider at the lower end than at the upper end (Su et al., 2020), the center position of the plane was placed  $5^\circ$  below the central axis of the scene camera or, more precisely,  $5^\circ$  below the optical axis of the pinhole camera for rendering.

To measure the gaze data, we asked each participant to gaze at each marker for 3 s. Throughout the measurement, only one black marker appeared on the plane. When the participant pulls the trigger on the HTC Vive controller, a beep sound counts down for 3 s. The participants were asked to gaze at the marker during the beep. At the end of the beep, the marker jumped to a pseudo random position, and a new trigger pull started the beep. Each participant repeated this 25 times. As a result, we acquired 25 sets of gaze data for each participant. To estimate and evaluate the reliability of the marker gazing data, we used the middle 1 s out of the 3 s. Fig. A3 shows the positions of the displayed markers. Sixteen of the twenty-five sets (black crosses in Fig. A3) of gaze data were used for the estimation of the visual axis, and the other nine sets (red crosses in

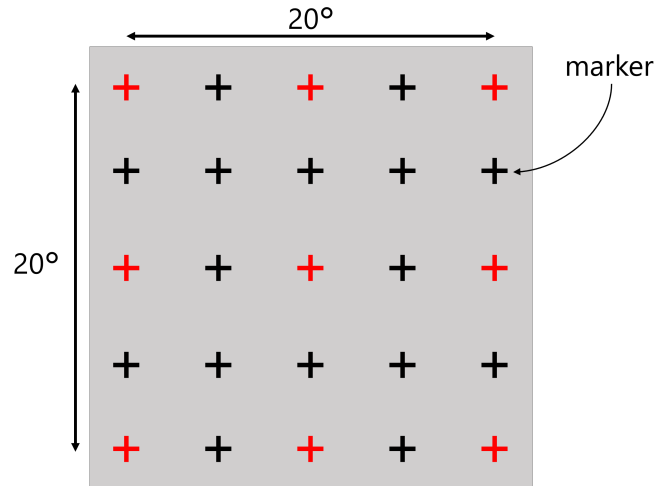


**Figure A3**

*Marker positions for the traditional calibration. Black crosses represent the markers used to estimate the visual axis. Red ones were the markers used to evaluate calibration parameters. Actually, the markers were presented one by one in black color. All the markers were displayed within a viewing angle of 20°.*

Fig. A3) were used for the evaluation of the calibration parameters.

### Calibration Error

This section explains the regression model for estimating the visual axis using 16 markers and the method for evaluating the accuracy of the calibration parameters using nine markers. The visual axis was estimated to minimize the sum of squared distances between each marker and its points of regard (PoRs) on the plane using the following first-order polynomials (White et al., 1993):

$$u_{\text{vis}} = a_1 + a_2 u_{\text{raw}} + a_3 v_{\text{raw}}, \quad (\text{A1})$$

$$v_{\text{vis}} = b_1 + b_2 u_{\text{raw}} + b_3 v_{\text{raw}}, \quad (\text{A2})$$

where  $[u_{\text{raw}}, v_{\text{raw}}, 1]^T$  is the raw gaze direction after calibration using the tool of the head-mounted display.  $[u_{\text{vis}}, v_{\text{vis}}, 1]^T$  is the visual axis as the control condition.

Fig. A4 shows the gaze directions after the first calibration (raw gaze direction in Fig. A1)

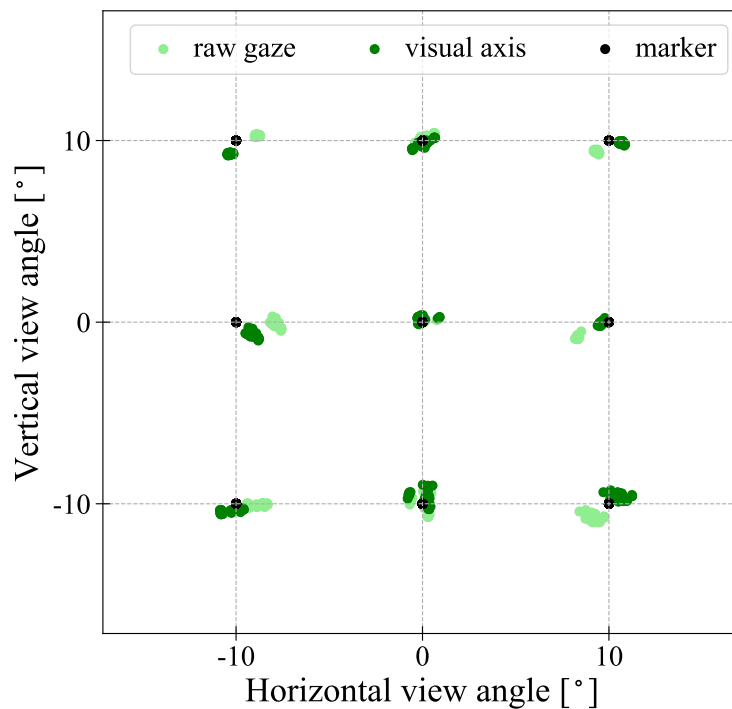


**Figure A4**

*PoRs of raw gaze direction and visual axis for markers. The light green and green points indicate the PoRs of the raw gaze direction and visual axis on the plane where markers are displayed, respectively. The black points represent marker positions.*

and the gaze directions after the second calibration (visual axis in Fig A1) when gazing at the nine markers for evaluation. Because the human gaze fluctuates, even with the visual axis, which is the control condition, has errors. This is why we separated the markers necessary for estimating the regression model parameters from those required for evaluating the calibration parameters, similar to machine learning where training data and evaluation data are separated. For evaluation, nine sets of gaze directions were calibrated using the parameters of the regression model or the 3D eye model used in the proposed method, and the average absolute error between the markers and the visual axis or the calibrated gaze directions was computed in degrees. In Fig. A4, for example, the error with the raw gaze direction was  $1.02^\circ$  and that with the visual axis was  $0.65^\circ$ .